TECHNISCHE UNIVERSITÄT WIEN
Vienna University of Technology

MASTER THESIS

Synthesis and characterisation of anisotropic metal chalcogenide nanomaterials

submitted to the

Institute for Applied Synthesis Chemistry

of the Technische Universität Wien

Supervisor

Univ.Prof. Dipl.-Ing. Dr.techn. Wolfgang LINERT

by

Rolanda RATKIC, 00912149

Stöbergasse 17/14, 1050 Wien

Wien, July 2018

Ratkic Rolanda

Abstract

The desire of controllable size and shapes with different nanomaterials is motivated because of their properties and resulting applications. Due to the large amount of surface atoms, nanomaterials differ from their bigger counterparts. Properties like the melting point, electric conductivity, optical characteristics or general chemical activity of a molecule change.

This thesis uses an efficient ‘hot injection’ approach synthesis in oleylamine producing anisotropic two-dimensional nanomaterials. The solvent oleylamine additionally acts as stabilizer and reducing agent. Various metal-chalcogenide nanomaterials are produced with different sizes and shapes. The chalcogenides, sulphur and selenium, were reduced to sulphide and selenide in oleylamine. The metal salts used ($CuCl_2*2H_2O$, $FeCl_2*4H_2O$, $FeCl_3*6H_2O$ and $NiCl_2*6H_2O$) were dissolved in NMP beforehand and afterwards added to the stirring hot oleylamine-chalcogen mix via ‘hot injection’.

This results in dark-green copper sulphide nanoplates, which are getting smaller with decreasing temperature and are clearly seen in TEM images. These nanoplates were measured with XRD and show a clear hexagonal pattern. Optical measurements such as UV-VIS show a plasmon and a band gap absorption, which could be used in sensor applications. Apart from that black copper selenide nanowires, and with increasing temperature, triangular copper selenide nanoplates have been produced. TEM images were taken and optical measurements show band gap and plasmon absorption as well. XRD measurements show a face centred cubic pattern. Furthermore, dark-brown iron sulphide and black iron selenide nanosheets as well as nickel selenide nanoscrolls have been produced. Depending on which iron-salt educt (Fe[II]-salt or Fe[III]-salt) has been used, sizes of the nanosheets vary. TEM pictures were taken of all nanomaterials and the XRD measurement of the iron selenide nanosheets show an orthorhombic pattern.

Kurzfassung

Nanomaterialien in verschiedenen Formen und Größen sind wegen ihrer vielfältigen Eigenschaften und daraus resultierenden Anwendungen ein viel erforschtes Gebiet. Wegen ihrer hohen Anzahl an Oberflächenatomen, unterscheiden sich Nanopartikel von größeren Materialien. Eigenschaften, die sich ändern sind beispielsweise der Schmelzpunkt, die elektrische Leitfähigkeit, das optische Verhalten wie auch die generelle chemische Aktivität eines Moleküls.

Diese Arbeit bedient sich einer ‚hot injection' („Heißeinspritztechnik") Technik, bei dem das Lösungsmittel Oleylamin verwendet wird, welches zusätzlich als Reduktions- und Stabilisierungsmittel dient. Es werden dabei verschiedenste Metall-Chalkogene Nanomaterialien mit unterschiedlichsten Größen und Formen, sowie Zusammensetzungen hergestellt. Verwendete Chalkogene sind Schwefel und Selen, welche in Oleylamin zu Sulfid und Selenid reduziert werden. Die verwendeten Metallsalze ($CuCl_2$*$2H_2O$, $FeCl_2$*$4H_2O$, $FeCl_3$*$6H_2O$ und $NiCl_2$*$6H_2O$) wurden zuvor in NMP gelöst und danach via ‚hot injection' Technik zum heißen rührenden Oleylamine-Chalkogen Gemisch injiziert.

Daraus resultierten dunkelgrüne Kupfersulfid Nanoplättchen, welche durch TEM Bilder eindeutig erkennbar sind und bei sinkender Reaktionstemperatur kleiner werden. Diese wurden mit XRD gemessen und weisen auf eine eindeutige hexagonale Struktur hin. UV-VIS Messungen zeigen eine Plasmon Absorption, sowie eine Bandlückenabsorption, diese Eigenschaften könnten zum Beispiel bei Sensoren angewandt werden. Außerdem wurden schwarze Kupferselenid Nanodrähte sowie dreieckige Nanoplättchen durch Temperatur Erhöhung hergestellt und mittels TEM Bilder erstellt. Die Nanoplättchen weisen auch auf Bandlücken- und Plasmon Absorption hin und die Kristallstrukturanalyse (XRD) ergibt kubisch-flächenzentrierte Kirstallstruktur. Darüber hinaus wurden dunkelbraune dünne Eisensulfid und schwarze Eisenselenid Nanoblätter, unterschiedlicher Größe je nachdem Fe(II)-Salz oder Fe(III)-Salz als Edukt verwendet, sowie schwarze Nickelselenid Nanorollen hergestellt und mittels TEM Bilder angefertigt. Die Eisenselenid Nanoblätter ergeben durch die XRD-Messung eine eindeutige orthorhombische Kristallstruktur.

ACKNOLEDGEMENTS

First and foremost, I would like to thank my supervisor Univ.Prof. Dipl.-Ing. Dr.techn. Wolfgang Linert of the Technical University Vienna, for providing me the opportunity to work on my master thesis at Trinity College in Dublin via Erasmus. His assistance and advice have been very much appreciated and have guided me throughout my time working on this research project.

Furthermore, I would like to express my gratitude to Prof. Dr. Iouri Gounko from Trinity College Dublin for letting me work in his laboratory and for giving me such an interesting topic to work on. I also thank him for the opportunity to work with such great laboratory equipment such as the Transmission Electron Microscope.

Special thanks to Dr. Sarah McCarthy, from Trinity College Dublin for her support during my laboratory work. She helped me both in the laboratory and with the measurements. She taught me so much and I was very happy that I could contribute to her Nature publication. I also thank David Muñoz García for making the daily lab-life much more fun!

Finally, I would like to thank my parents, who always supported me emotionally and financially. Without them I would have never been able to study in the first place. My deepest gratitude goes to my boyfriend Jonathan Norris for his assistance and mental support during the time I worked on this thesis as well as my friends for all the encouragement.

ABBREVIATIONS

ATR FTIR……..Attenuated total reflection fourier-transform infrared spectroscopy

CCP……..……Cubic close packing

HCP……..……Hexagonal close packing

NMP……..N-Methyl-2-pyrrolidon

OAm……Oleylamine

TEM……Transmission electron microscopy

Vs……Symmetric stretching vibration

Vas……...Asymmetric stretching vibration

δ……Bending vibration

UV- VIS……Ultraviolet and visible spectroscopy

XRD……X-Ray Diffraction

Table of Content

1. Introduction and Aims of the Thesis

Already in 1959 Richard Feynman said in his famous lecture "*There is plenty of room at the bottom*" (Feynman, 1960) that it would be possible to build matter atom by atom. With this speech he laid the foundation for the development of nanotechnology [2]. It became a vibrant research area and has had a big impact in many fields in today's world. The reason for this immense interest on nanoscale materials, which have a size range from 1 nm to 100 nm according to the *International Organization for Standardization* (ISO), is their physical and chemical properties, which differ from their bulk state counterparts [3] [4] [5]. The properties vary not only with different materials, but also when it comes to shapes, sizes and crystalline structure [6]. Their high surface area benefits them for example when it comes to reactivity as catalytic reactions occur on surfaces. Therefore it is a fact that nanosized materials are generally more reactive than large particles with the same mass [7]. Many areas have benefited from the progress of nanotechnology including electronics, energy harvesting, drugs and medications among many others. Hence, applications in these fields require precisely defined particles [8].

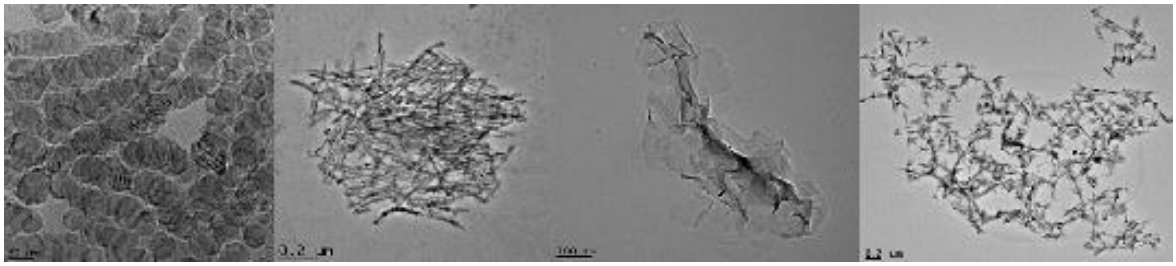

Figure 1: CuS nanoplates, CuSe nanowires, FeS nanosheets and NiS nanoscrolls

Nanomaterials can be polymers, semiconductors, metals or ceramics, having a structure of single or multiple crystalline, quasicrystalline or amorphous phases [9]. However, this thesis focuses on semiconductors only, considering that the continuous electron band is changed with nanosized materials and therefore resulting in a higher thermal conductivity [10]. On the surface larger amounts of atoms appear which lead to a lower melting point because the surface energy increases. Unsaturated sites and less adjacent coordinate atoms let the particles in general be more chemically active [11].

The aim of this thesis is to tailor different metal chalcogenide nanomaterials having as much different morphology as possible using an adaptable hot injection approach in oleylamine (OAm) [2] [12]. Optimizing kinetic conditions to synthesise anisotropic nanomaterials which are uniform, consist of different shapes, sizes and compositions. The conditions vary between the reaction time, the temperature, the concentration, precursors and an optimised purification strategy. Additionally to simplify the hot injection synthesis N-Methyl-2-pyrrolidon (NMP) was used [12]. Once an optimum reaction was found, reproducibility was tested.

Figure 1 shows that different semiconductors have been produced. Besides CuS nanosheets, $Cu_{2-x}Se$ nanowires, FeS nanosheets and NiSe nanoscrolls, also $Cu_{1.8}Se$ nanoplates as well as $FeSe_2$ nanoplates have been produced. The structure characterization, as well as the characterization of the absorption spectra, morphology and composition were done with Transmission electron microscopy (TEM), Energy-dispersive X-ray spectroscopy (EDX) Attenuated Total Reflection Fourier-Transform Infrared Spectroscopy (ATR-FTIR), X-ray diffraction (XRD) and UV-VIS absorption spectra [13].

2. Theoretical Background

The basics of nanotechnology are that besides the variation of the chemical composition of materials, also the size and arrangements of the particles are important. This leads to a change of the physical and chemical properties, which is precisely why structuring of substances or materials is one of the most important aspects in nanotechnology [14] [15].

2.1 Classification of Nanomaterials

In the last years, hundreds of novel nanomaterials have been developed. They are classified into four categories: 0-dimensional, 1-dimensional, 2-dimensional and 3-dimensional [16].

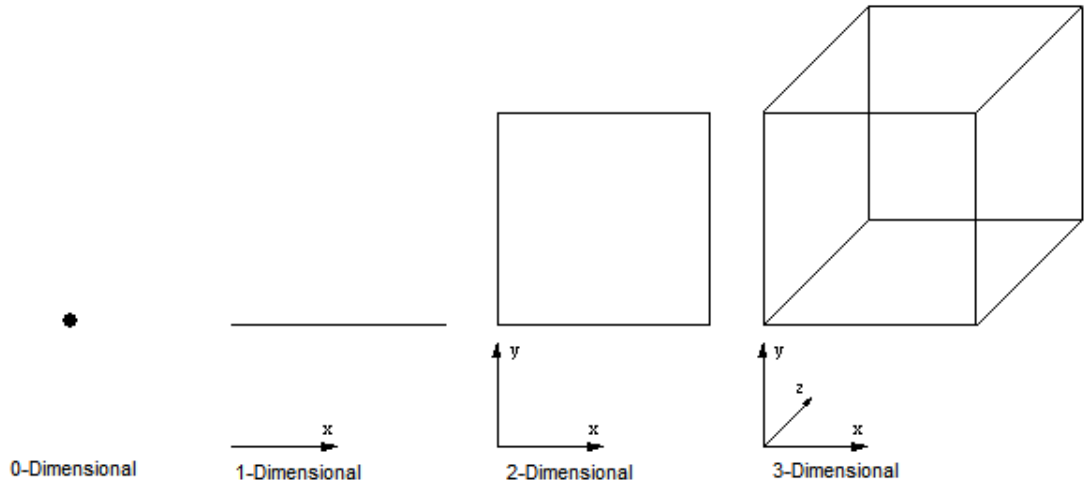

Figure 2: Classification of Nanomaterials

In Figure 2 0-dimensional nanoparticles are shown, which are basically large atom clusters, whose excitons (electron-hole pairs) are confined in all the three directions. 1-dimensional materials have layered or lamellar structures, where only the layer is nanometres thick. 2-dimensional materials are filamentary structures where its diameter is in the nanometre range. 3-dimensional nanoparticles are most common and have all three dimensions in nanometre size [9] [17] [18].

Table 1: Nanomaterial examples of the 4 dimensions [19]

0-dimensional nanomaterials	1-dimensional nanomaterials	2-dimensional nanomaterials	3-dimensional nanomaterials
quantum dots	thin films	nanofibers, nanowires, nanotubes nanosheets	nanoparticles, dendrimers, nanocapsules, fullerenes, etc

Table 1 shows some typical examples of shapes of nanomaterials of the 4 dimensions. The following are examples of some shapes explained in detail.

2.1.1 Quantum dots

Quantum dots have a particle size from 1 nm to 10 nm and their energy levels can be measured spectroscopically [14]. Studies found that zero-dimensional nanomaterials like quantum dots are high quality field emitters. *Van Haesendonck et al*. synthesised ZnO quantum dots and field emission measurements exhibited good results. Application devices for electron field emitters are broad, from a flat panel displays, to microwave amplifiers, to electron beam microscopes etc [20].

2.1.2 Thin films

One dimensional thin films are either produced through a chemical deposition (CVD) like a gaseous phase, a liquid phase or a solid phase, or from a physical deposition (PVD) such as sputtering technique, ion plating or MBE. Applications are in semiconductor technology, such as in solar cells, but also for laser diodes, quantum cascade lasers and so on. [19]

2.1.3 Nanowires

Nanowires are two dimensional and formed by self-assembly. Either they are ultrafine wires or linear dots. The range of materials is wide, from silicon, to gallium nitride or indium phosphide. Applications of nanowires are semiconductors, high data storage, electronic devices etc. They have exceptional properties such as magnetism or optical and electrical characteristics [21]. It is also important to mention that because of the high length to diameter ratio of nanowires, the field emission is exceptionally good [20].

2.1.4 Nanotubes

Nanotubes are based on layered compounds which are rolled up and two dimensional. When it comes to applications they are promising because of their exceptional properties. The best example are carbon nanotubes. They have tribological properties, as well as catalytic reactivity, a high receptivity for hydrogen and lithium and are resistant to shockwave impacts [9] [21].

2.1.5 Nanoscrolls

The two dimensional nanoscrolls are very similar to nanotubes, but they have a rolled up spiral like geometry and open edges at the end [22]. Carbon nanoscrolls are the most common ones and there are plenty of methods to produce them, including high energy ball milling, arc discharge or intercalation. Though due to their difficult colloidal processing, there are not many applications with this particular shape [23].

2.1.6 Nanosheets

Nanosheets are also two dimensional and have a thickness from 1 – 100 nm. The most common example is graphene. The carbon nanosheet is the thinnest and consists of a single layer with a hexagonal lattice [24]. There are also many other different materials forming nanosheets as for example described from Qurashi et all. GaON nanosheets are produced with a sonochemically assisted solvothermal process. They have interesting optical properties and a potential application could be as a photocatalyst in water splitting [25].

2.1.7 Nano dendrimers

Three dimensional nano dendrimers are complex multifunctional polymers with a diameter of 1-10 nm. It has a core and from that point it branches out like a tree. They are produced through emulsion polymerization and their applications depend on what materials are used. For example in nanolatex, coloured glasses, sensors, electrodes, pharmaceuticals etc [26].

2.2 Nanocrystal growth

To build an exact shape of a material it is necessary to understand the growth mechanism of different synthesis conditions. Formable shapes must be predicted under certain conditions. Therefore, the thermodynamic and kinetic shape control has to be considered [27]. Besides the reciprocity of kinetics and the anisotropy, as further explained underneath, thermodynamics is a key aspect in the inorganic crystal morphology. Because of the chemical bonding theory the thermodynamic morphology is foreseeable. When a reaction is controlled thermodynamically the result is a round shape. This happens because the growth rate is slower and unidirectional. Under kinetic conditions crystal growth is much faster. However, these kinetic conditions like the impurity, temperature or the choice of the solvent depend on chemical routes and conditions. Certain facets grow faster than others, therefore an anisotropic shape is the result. Also twinning and stacking faults in the initial crystal seed should be considered as partly responsible for forming a crystal shape. While there is so much research on crystal growth, there are still challenges to systematically control crystal morphology [12] [28].

2.2.1 Anisotropy

Anisotropy is the tendency of molecules and materials to exhibit variations in physical properties along different molecular axes (different direction) of the substance. These physical properties can be for example the electric- or thermal conductivity, polarizability or magnetization. For example, the graphite conductivity is bigger in the horizontal direction than in the perpendicular direction. It is a known fact that optical properties are especially dependent on the shape of the crystal. All crystals show anisotropy, however isotropic materials for example glass have the same properties for all directions [29] [30]. Figure 3 shows an anisotropic crystal, where you can see the different directions.

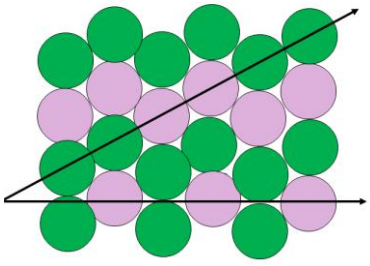

Figure 3: Anisotropy of a crystal, different directions shown

Because of this wide variety of properties, it has drawn a lot of attention to synthesise anisotropic metal nanostructures in the last decade. The advantages in areas of anisotropic to isotropic shapes are for example in energy harvesting, nonlinear optical responses, polarized light absorption, as well as many others [12].

2.2.2 Crystallographic defects

All real crystals with a thermodynamic equilibrium have defects. An ideal crystal with atoms ordered and resting at their perfect lattice position could only exist at absolute zero. These disturbances occur because atoms vibrate, and systems attempt to increase their entropy (ΔS). The entropy which increases is the configurational entropy and is defined by the Boltzmann equation in equation 1.

Equation 1: Boltzmann equation

$$S = k\ lnW$$

K is defined as the Boltzmann constant and W is the probability and is proportional to 10^{23}.

Equation 2:Gibbs Free Energy

$$\Delta G = \Delta H - T\Delta S$$

As equation 2 shows, when the entropy (ΔS) and the temperature (T) increases the enthalpy (ΔH) decreases and consequently the Gibbs Free Energy (ΔG) also decreases. So, the higher the temperature and the entropy, the more defects are in a system. With every temperature an equilibrium of defects can be built up with a Gibbs Free Energy as small as possible. And even if the defect concentration is extremely low, the lattice symmetry is broke, but in practice small defects are without consequences. There are numerous defects, most notably point defects like the Schottky defect or the Frenkel defect, solid solutions or dislocated and mechanical properties of solids. However in this thesis only extended defects like stacking faults and twinning will be described a bit more in detail because they play a role in shaping the materials [14] [15] [31].

2.2.2.1 Stacking faults

In a layered crystal structure stacking faults are most common and are caused by an interruption of the normal stacking sequence by ‘wrong’ layers. It occurs especially in 2 dimensional materials and in the two main polytypes ccp and hcp. A normal stacking sequence can be ABCABCABC etc. and if there is a stacking fault it can occur like an irregularity such as ABCACABC. The energy these defects carry is called stacking fault energy. [31] [32] [33]

2.2.2.2 Twinning

Crystal twinning is a phenomenon that occurs when two or more separate crystals of the same material originate from the same symmetrical lattice point. The first crystal is related to its unit cell by a symmetry element. The amount of directions the growth will occur is determined by the shape of the nanomaterial. Resulting in intergrowing of the crystals. However, if two crystals with a different structure grow together it is not twinning. According to the model of nucleation the stacking fault energy is related to the stress of twin nucleation. They are distinguished in two categories, the crystals where some reciprocal lattice points contain contribution from one twin only and crystals where all points contain contributions from both twins. Magnetic point groups are helpful for analysing twins and symmetry elements are shown via the miller index. With diffractometers like X-rays, every twin will show a different diffraction pattern. [12] [32] [34] [35]

2.3 Properties of Nanomaterials

The attention is now turned to the question of what reason a chemical compound or an atom changes its intrinsic properties because of the change of their sizes. Most crystals have cubic or hexagonal close packing (ccp and hcp) of atoms, in which a central atom is surrounded by twelve other atoms. Figure 4 shows hcp and ccp, the dashed lines in the hcp and the black lines in the ccp are the layers above.

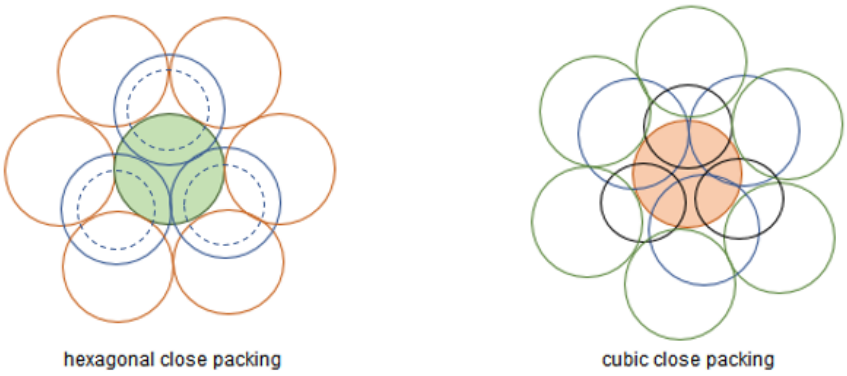

Figure 4: hexagonal close packing and cubic close packing

With a particle of 13 atoms which has a diameter smaller than 1 nm, surface atoms would be 90 % of all the atoms. In bigger crystals the surface atoms make only a tiny percentage of all atoms. Their properties are defined by their bulk, which are atoms inside the crystal. Even properties of particles of the size of 1 nm to the size of 10°nm are different because the ratio of the surface atoms and the atoms on the inside change. The smaller the particles, the more of the particles' atoms are on the outside. Atoms in the inside of a crystal are more strongly bonded and are almost only surrounded by adjacent atoms. Surface atoms are only partly surrounded by adjacent atoms and therefore they are not so strongly bonded. The high percentage of surface atoms has a strong influence on a materials property [14] [15] [31]. The following are some examples for properties of nanomaterials explained in detail.

2.3.1 Melting point of nanomaterials

The melting point is a physical constant where a material turns from solid into liquid, depending on the strength of the atom or ion bond. [36] However, this constant only counts if the number of atoms on the inside dominates and the surface atoms are insignificant. Smelting starts with the oscillation or displacement of weaker bonded surface atoms, whereby inner atoms come to the surface. The melting point is reached when the order of a material is destroyed. Therefore, this changes with nanomaterials due to their high amount of surface atoms. With decreasing particle size, the melting point also decreases. Hence lower temperatures are needed to work with nanomaterials. [14] [15]

2.3.2 Electric conductivity of nanomaterials

Linear decreasing of specific conductivity with increasing temperature is characterized as metal behaviour. It is explained with the scattering of moving electrons because of lattice vibrations and lattice defects. Conductive properties are explained with the band gap structures. Materials with a metal conductivity have partly occupied conduction bands and free movable delocalized charge carriers. With decreasing particle size, the energy bands decrease, and the number of delocalized charge carriers gets smaller. That is the reason why electric conductivity of nanomaterials with decreasing particle size reduces. Particles with a size smaller than 30 nm have negligible scattering for visible light and therefore they are used as a transparent conductor. [14] [15] [37]

2.3.3 Optical properties of nanomaterials

Already in the 19th century, Michael Faraday discovered the optical properties of small materials. A solid material with a band gap is transparent for visible light until a certain energy. Only when the energy beam is bigger than the band gap an electron is transferred to the conduction band by absorption of a photon. Leaving behind a positive charge in the valence band. If the excited electron recombines with the positive charge when falling back, fluorescence radiation is emitted. The emission colour of a material depends on the size of the bandgap and is for big sized crystals a constant. Nanosized semiconductors increases their band gap the smaller the particle. If the bandgap is in the region of visible light, the colours of the materials change only by changing the size of the particles. Therefore, you can produce pigments in all the different spectral colours only by changing the size of the particles. These finite-size effects are used in many

applications, like for example in biological systems by tying them to DNA or enzymes. But they are also used for lasers, diodes or displays. [9] [14] [15]

2.3.4 Surface chemistry and catalysis

As mentioned before with decreasing particle size the number of surface atoms increases and the percentage of inner atoms gets smaller. With surface active substances the ratio of surface to volume as a function of the particle size is considered. Surface atoms have smaller coordination numbers than inner atoms and therefore free coordination sites for reactions. They are chemically more reactive and more soluble. Due to their big surface, nanomaterials are extremely efficient in reactions with gases, solids and liquids. This is also explained due to the higher energy of the surface atoms. And because of the different surface functionalities of different materials lots of diverse applications, like in catalysis or self-cleaning of surfaces, are possible. [14] [15]

2.4 Transition metal chalcogenides

In general chalcogenides are the 6th main group of the periodic table and consist of oxygen, sulphur, selenium, tellurium and polonium. Chalcogen is Greek and means ‘ore former’ because of oxides and sulphides they are literally involved in the setup of ores. Accordingly, to their electron configuration s^2p^4 they take two electrons to reach their noble gas configuration. That is why the oxidation state [-II] is preferred. Sulphur or selenium chemically bonded with metals become sulphide or selenide with the oxidation state [-II]. [38] [39]

Transition metal chalcogenides are a large family and chalcogenides have a large range of physical properties like, superconductors, semiconductors, metals, semimetals, insulators. Semiconductors are layered materials, have a strong covalent bonding, but a week Van-Der-Waals interaction in between the layers. It is easy to peel them into a mono layer so that it becomes a direct band gap material. [40] Following are some examples of properties and applications of the produced metal chalcogenide nanomaterials.

2.4.1 Copper sulphide

Copper sulphide nanoparticles are among other things used for the photo thermal ablation of cancer cells. The good thing of using these nanoparticles is that they can be directed selectively to the cancer cells and have many advantages for example low production costs and low cytotoxicity [6]. Another example are CuS nanorods and nanowires sensing food pathogens, small molecules and immunologically relevant moieties [3].

2.4.2 Copper selenide

Copper selenide nanocrystals can be used in photothermal therapy as shown from *Korgel et al*. They produce photothermal heating, when excited by light with a wavelength 800nm. This property was used in vitro to destruct cancer cells [41]. Another example are its enhanced electronic properties, as explained from *Prieto et al*. The particles have conducting and semiconducting properties depending on the layer and could be used in optoelectronic devices. [41]

2.4.3 Iron sulphide

Most notably are the magnetic properties of iron chalcogenide particles. *Mei Liu et al*., describe a synthesis to produce ferromagnetic FeS nanowires which even became superparamagnetic when decreasing the size of the particles [42]. But besides that there are plenty of other applications with FeS as like biological electron transportation, redox potential modification or proton/electron transfer coupling [43].

2.4.4 Iron selenide

In contrast to FeS there are only a few reports on FeSe. In β-FeSe superconductivity had been discovered [44]. The two-dimensional layered crystal structure was produced with a thickness of 2-3 nm by *WuMK et al*, in 2008 [45]. But besides that FeSe show as well photocatalytic activity and electrocatalytic activity as amperometric sensors [46].

2.4.5 Nickel selenide

Nickel selenide nanomaterials are known for their optical properties. Thin NiSe films are used for solar cell devices because of their low absorbance and high transmittance, resulting in a high absorption coefficient [47].

2.5 Synthesis of Nanomaterials

2.5.1 ‘Top Down’ and ‘Bottom Up’ Methods

Small gold particles have already been produced since the mid-19th century. For example, red church windows are made of gold nanoparticles which give them their colour [14]. Today the synthesis of nanomaterials are divided into two categories: ‘top-down’ and ‘bottom up’ methods as shown in figure 3. [48]

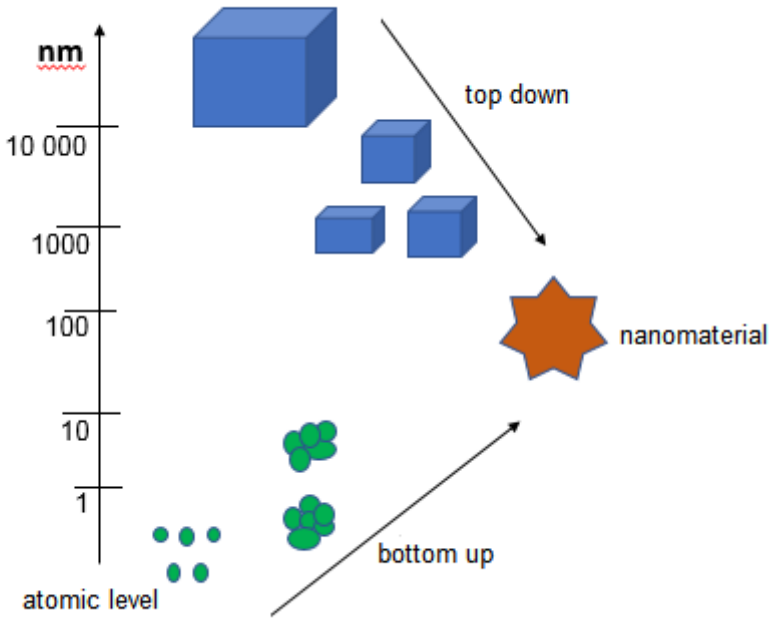

Figure 5: Top down and bottom up approach

The definition ‘top down’ refers to reducing from a large scale to a nanoscale. A milling process is used to reduce the size mechanically. In contrast ‘bottom up’ methods are building up nanomaterials by chemical processes. These processes can be aerosol processes, like flame hydrolysis or spray hydrolysis, but also processes in liquid phase. For example, the sol-gel process, the precipitation process, micro-wave-assisted synthesis or thermal processes like hydrothermal reactions. Recently also nanomaterials were produced in reactions in organic solutions. Both techniques, ‘top down’ and bottom up’ have its advantages and disadvantages. Depending on the wanted composition either ‘top down’ or ‘bottom up’ approaches are used. [8] [48] [49]

2.5.2 ‘Hot Injection Synthesis’

One of the most frequently used ‘bottom up’ methods is the ‘hot injection synthesis’. It is a thermal decomposition technique and forms highly crystalline, monodisperse nanomaterials also getting a reasonable yield. [12]

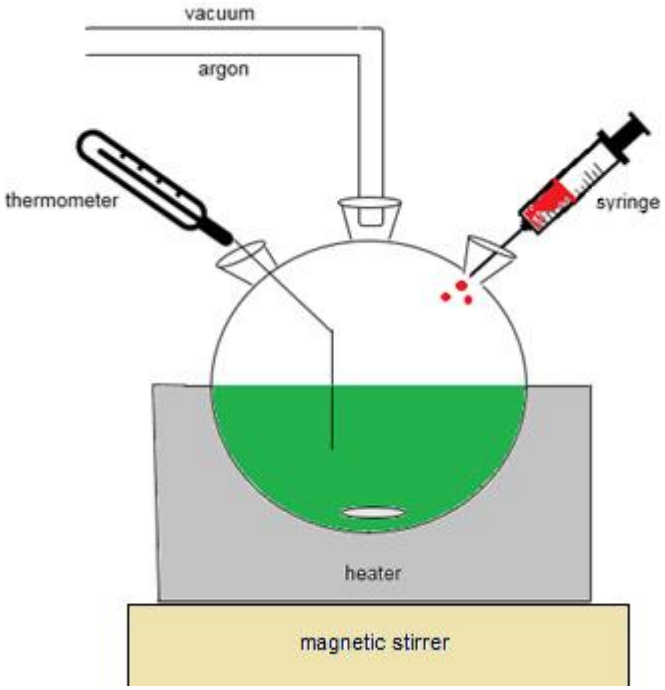

Figure 6 hot injection synthesis

At the ‘hot injection synthesis’, a cold dissolved precursor is quickly injected into a hot stirring mix of solvent and the other precursor. Resulting in a burst nucleation, followed by controlled growth to create monodisperse nanomaterials. Because the properties are changing with different material sizes as explained above it is very important to produce uniform particle sizes. This method is a clear break from former wet synthesis. Previous synthesis used precursors dissolved in water or other polar solvents. The advantages of the hot injection approach over hydrolytic ones is that it allows higher reaction temperatures up to the boiling point and gives an interaction environment for active metal atoms. Generally in contrast to the ‘hot injection’ method there is the ‘heat up’ approach, where the precursors are already mixed when still cold and afterwards heated up with an oil bath or heating mantle. [4] [49] [50]

2.6 Oleylamine (OAm)

A typical organic solution for a hot injection bottom up synthesis is oleylamine. It is an unsaturated fatty amine with a chemical formula of $C_{18}H_{35}NH_2$. This versatile reagent has a high boiling point and is proven to be efficient to produce several types of nanomaterials. [4] [51]

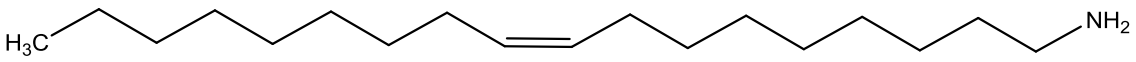

Scheme 1: Oleylamine

It is a chemical which acts in many ways. As a viscous solvent, reducing agent and a surface coordinated ligand. [12] It binds the semiconductor particles as an agent and thus prevents uncontrolled growth of the particles. Therefore it acts as a stabilizer [9].

Scheme 2 below shows the mechanism of sulphur reduced to sulphide (-II) by oleylamine producing a branched amidine.

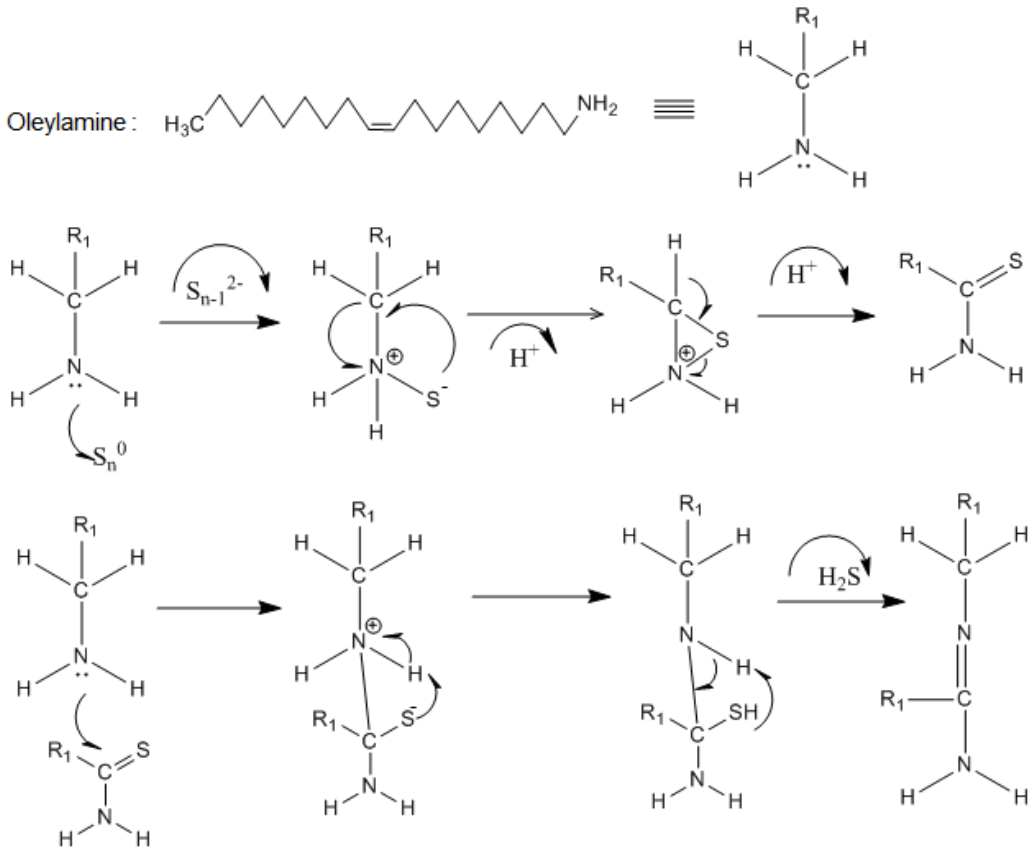

Scheme 2: Reaction of sulphur reducing to sulphide with oleylamine

Scheme 3 shows the reduction of selenium to selenide by oleylamine.

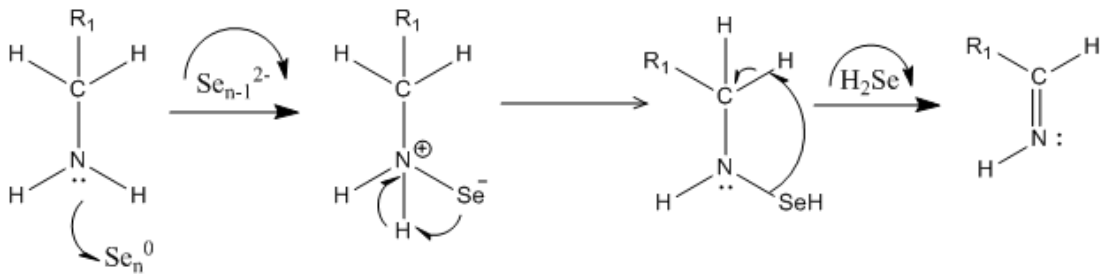

Scheme 3: Reduction of selenium to selenide with oleylamine

3. Results and Discussion

3.1 Copper sulphide (CuS)

The first syntheses were made with copper(II)dichloride dehydrate ($CuCl_2*2H_2O$) which was dissolved in NMP and added via 'hot injection' to a hot oleylamine-sulphide solution to react for 30 minutes. Beforehand sulphur (S^0) was reduced in degassed oleylamine to sulphide (S^{-2}) under inert conditions, which took approximately an hour at 80°C. As shown on the TEM pictures in figure 7, 8 and 9, three CuS products with different sizes were produced.

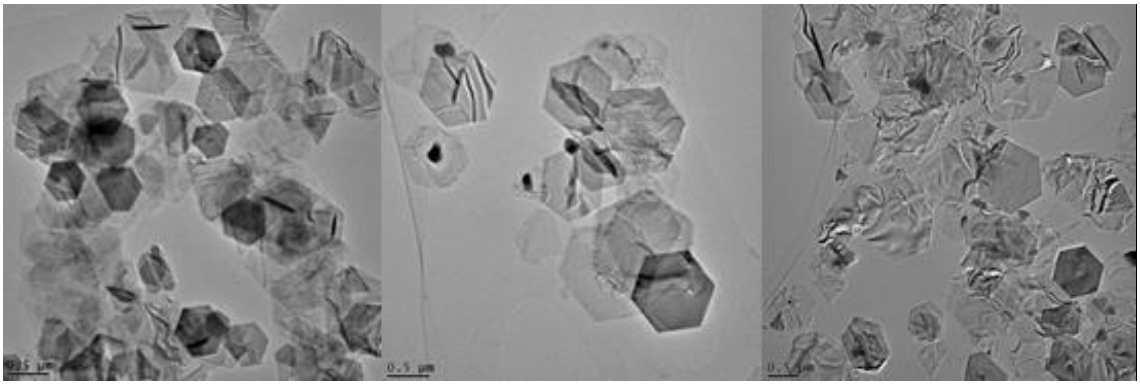

Figure 7: TEM images of CuS nanoplates; Product 1: reaction temperature 180°C;

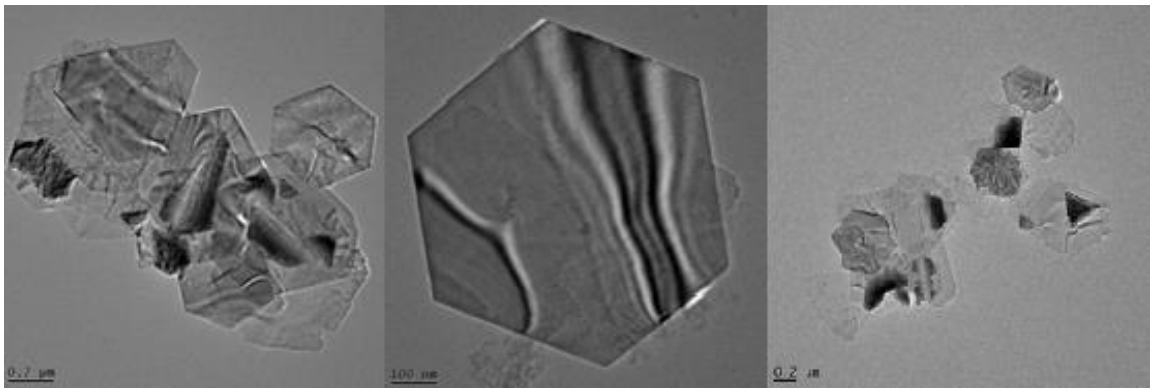

Figure 8: TEM images of CuS nanoplates; Product 2: reaction temperature 160°C

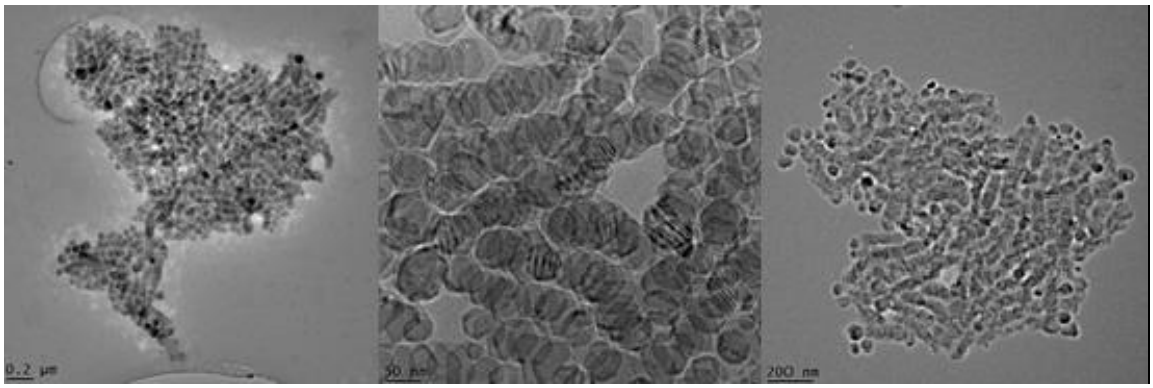

Figure 9: TEM images of CuS nanoplates; Product 3: reaction temperature 120°C

CuS nanoplates product 1, shown in figure 7, was reacting at 180°C in a concentration ratio of 1:3 mmol (Cu:S). The result was large, ultrathin, dark green, hexagonal and uniform copper sulphide nanoplates with the lateral length of 535 +/-119 nm. Product 2, shown in figure 8, was synthesized with 160°C and a concentration ratio of 1:2 mmol (Cu:S) resulting in smaller nanoplates. The lateral length of those hexagonal and as well green nanoplates is 408 +/-235 nm. Further experiments where done with even lower temperatures. However, reactions with temperatures at 150°C, 140°C and 130°C and a ratio of 1:2 mmol resulted in a mix of plates, sheets and impurities. Product 3 of the CuS nanoplates, shown in figure 9, was made at 120°C with a concentration ratio of 1:2 mmol resulting very small, green, uniform and hexagonal nanoplates lying upon another in a stacking arrangement. This is resulting because of their high uniformity and the lateral length is 49 +/-13 nm. The atomic ratio of the product 1 and product 2 of CuS is: copper: 55 % and sulphide: 45 % and product 3 shows an elemental ratio of: Cu: 52 % and S: 48 %. Figure 10 shows the EDX of CuS, which is the same for all 3 products. It contains copper twice at 0.9 and at 8 keV and a sulphur peak at 2.3 keV. There is a molybdenum peak because of the TEM grid.

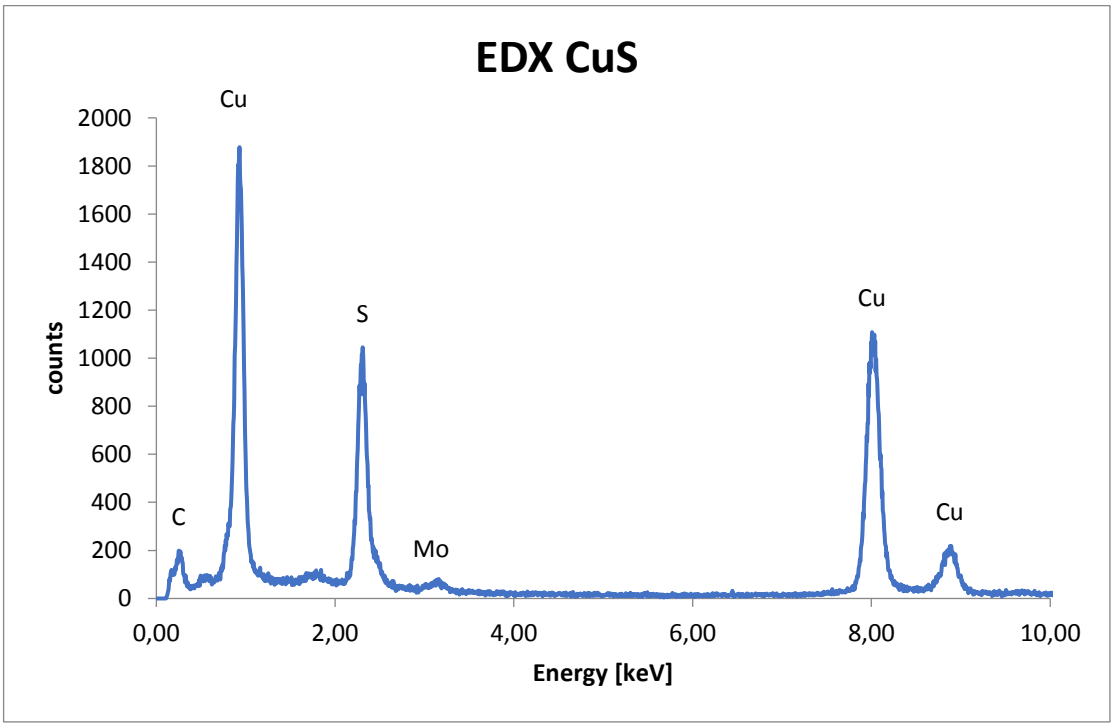

Figure 10: EDX CuS

The UV-VIS measurement of the three different CuS products are shown in figure 11. In all samples you can see the broad plasmon absorption towards the IR region and a band gap absorption below 400 nm, which is typical for CuS nanomaterials.

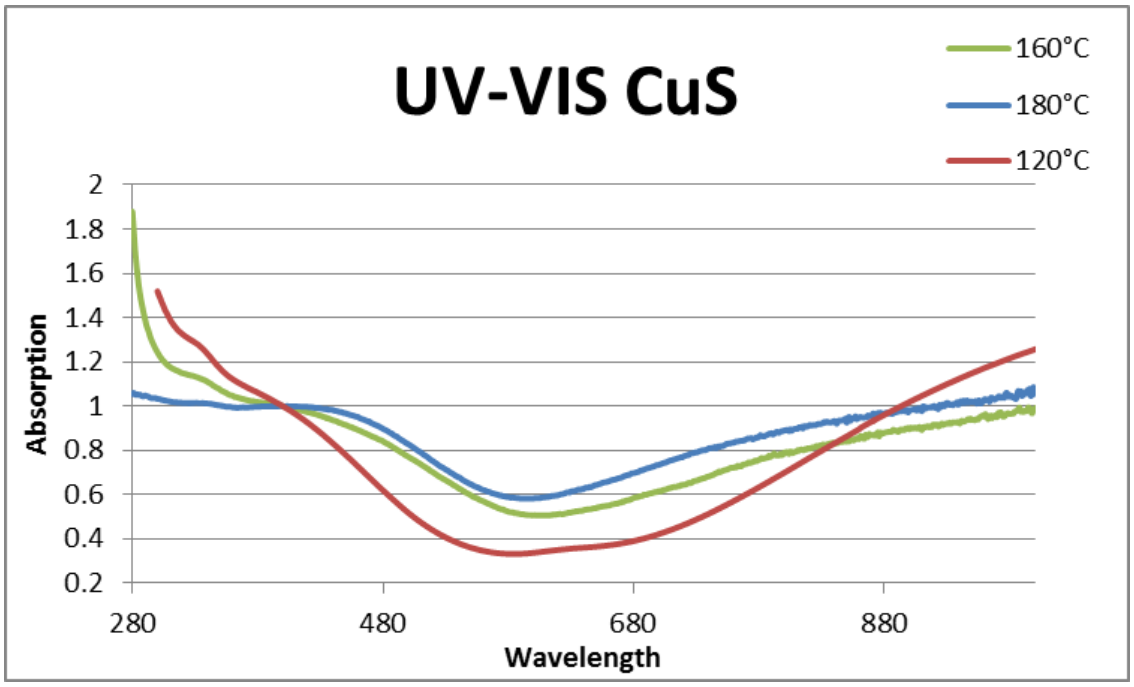

Figure 11: UV- VIS measurement CuS nanoplates

The ATR-IR measurements between 250 – 4000 nm of the three samples are displayed in table 2 and all three products show similar results. There are asymmetric (v_{as}) and symmetric stretching vibration (v_s) at 3300 to 3100 cm^{-1} of NH_2. There is a bending vibration (δ) of =C-H at 3000 cm^{-1}. An asymmetric (v_{as}) CH_2 vibration at 2920 cm^{-1} and a symmetric stretching CH_2 vibration (v_s) at 2852 cm^{-1}. And there are bending vibrations (δ) of –C=C at 1708 – 1673 cm^{-1}, of NH_2 at 1581 cm^{-1} and of CH_3 at 1460 cm^{-1}. These peaks give a definite proof that the oleylamine is still on the surface of the plates.

Table 2: ATR-IR CuS

Vibrational modes	Frequency (cm^{-1}) **Procut 1**	Frequency (cm^{-1}) **Product 2**	Frequency (cm^{-1}) **Product 3**
v_{as}(NH_2) and v_s(NH_2)	around 3351		3230-3126
δ(=C–H)	3000		
v_{as}(CH_2) and vs(CH_2)	2921, 2852	2921, 2854	2918, 2849
δ(-C=C)	1673	1708	1679
δ(NH_2)	1581	1588	1581
δ(CH_3)	1460	1466	1456
δ(C-N)	964	966	964

δ (C-C)	726		471

ν_s = symmetric stretching vibration; ν_{as} = asymmetric stretching vibration; δ = bending vibration

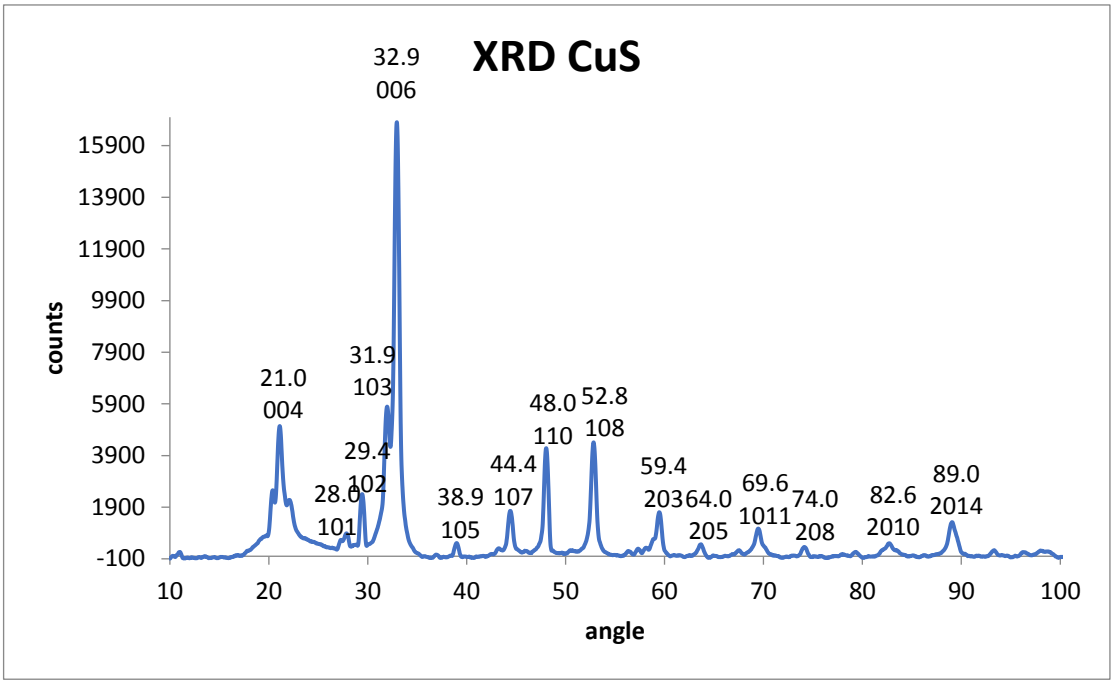

Figure 12: XRD CuS

Figure 12 shows the XRD of the CuS nanoplates. The pattern was compared to the file number 03-065-3561, a hexagonal CuS structure. The first diffraction point is at an angle of 21.0 and has parameters of (004), the next point is at an angle of 28.0 with the parameters (101) and another peak at an angle of 29.4 with the parameters (102). It continues at the angle of 31.9 with the parameters (103). And at the angle of 32.9 and the parameters of (006) the diffraction point is the highest and is a proof for anisotropy [12]. Other peaks are at an angle of 38.9 with parameters (105), 44.4 with the parameters (107), 48.0 with the parameters (110), 52.8 with the parameters (108), 59.4 with the parameters (203), 64.0 with the parameters (205), 69.6 with the parameters (1011), 74.0 with the parameters (208), 82.6 with the parameters (2010) and 89 with the parameters (1014). The XRD analysis proves for definite that the CuS nanoplates are hexagonal (hex).

3.2 Copper selenide ($Cu_{2-x}Se$)

In these reactions copper(II)dichloride dehydrate ($CuCl_2*2H_2O$) was dissolved in NMP and was added via 'hot injection' to a hot selenide-oleylamine solution. Beforehand selenium was reduced to selenide in degassed oleylamine under inert conditions, which took approximately five hours and was done mostly overnight. The selenium reduction needs higher temperatures (220°C) to fully reduce, unlike the sulphur reduction before. Two different $Cu_{2-x}Se$ products were produced as shown in the TEM pictures of figure 13 and 14.

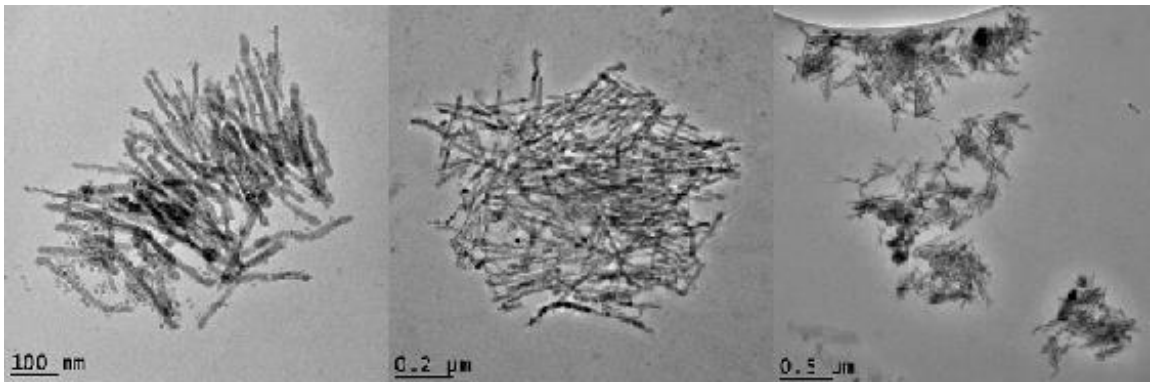

Figure 13: TEM images of $Cu_{2-x}Se$ nanowires; Product 1: 180°C

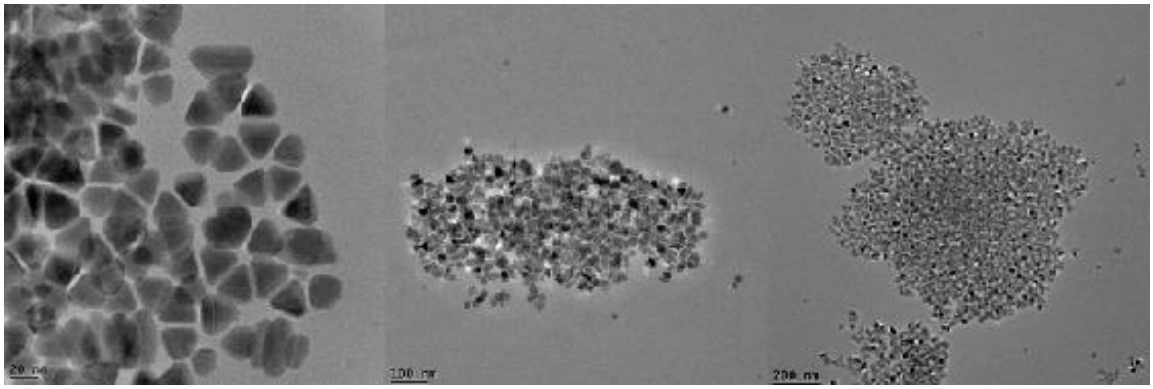

Figure 14: TEM images of $Cu_{2-x}Se$ nanoplates; Product 2: 210°C

Many different conditions of the reaction have been tried out. From verifying the temperature from 150°C – 220° to changing the reaction time from 30 minutes to 2 hours. Under the conditions of 180°C, a reaction time of 30 minutes and a concentration ratio of 1:2 mmol (Cu:Se) product 1 was produced as shown in figure 13. These large, black, uniform nanowires have the lateral length of 164 +/-64 nm. The 2nd product as shown in figure 14 was produced with a reaction time of 30 min, 210°C and a concentration ratio of 1:2 mmol (Cu:Se). Resulting in small black triangular nanoplates with a lateral length of 25 +/-11 nm.

Figure 15 shows the EDX of both $Cu_{2-x}Se$ products. Product 1 shows Cu peaks at 0.9, 8 and 8.6 keV and Se peaks at 1.4, 11.2 and 12.2 keV and an elemental ratio of Cu 60 % and Se: 40 %. Product 2 shows Cu peaks at 0.93, 8 and 8.9 keV and Se peaks at 1.4, 11.1 and 12.4 keV and an elemental ratio of Cu 65 % and Se: 35 %.

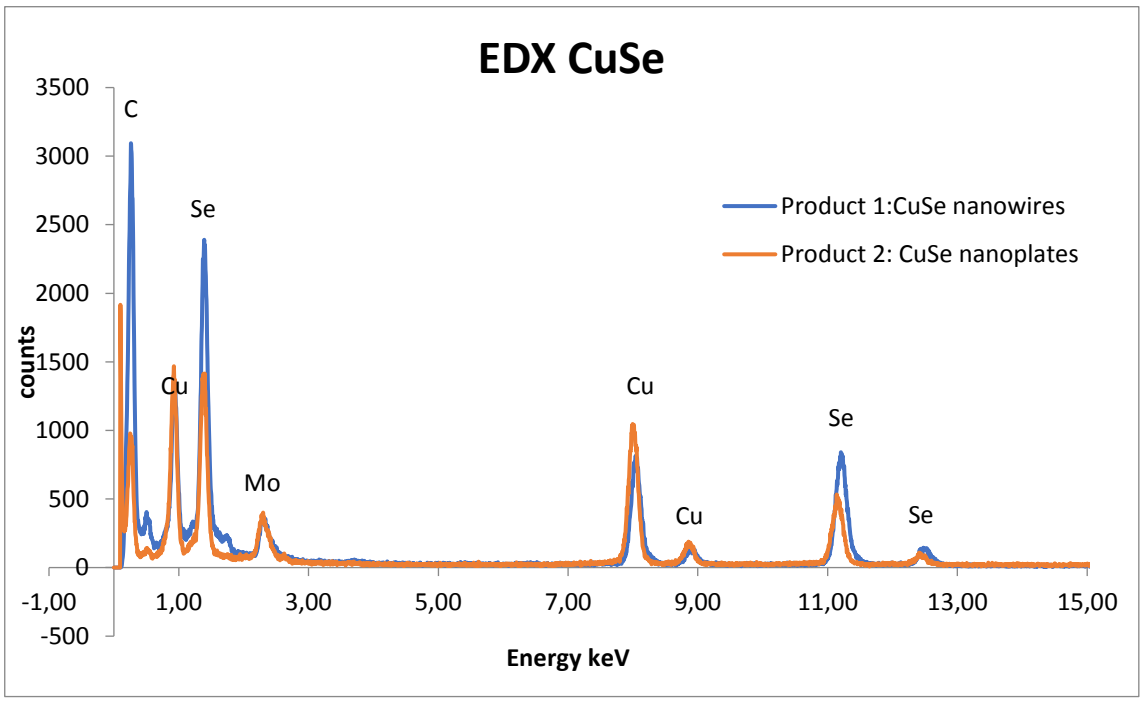

Figure 15: EDX $Cu_{2-x}Se$

Optical studies were made via UV-VIS measurements as shown in figure 16. The spectrum of the 1st product shows a broad shoulder at 280 nm which indicates to a band gap absorption. Product 2 has this band gap shoulder at 330 nm and gets another broad peak, starting at 780 nm which shows the plasmon absorption.

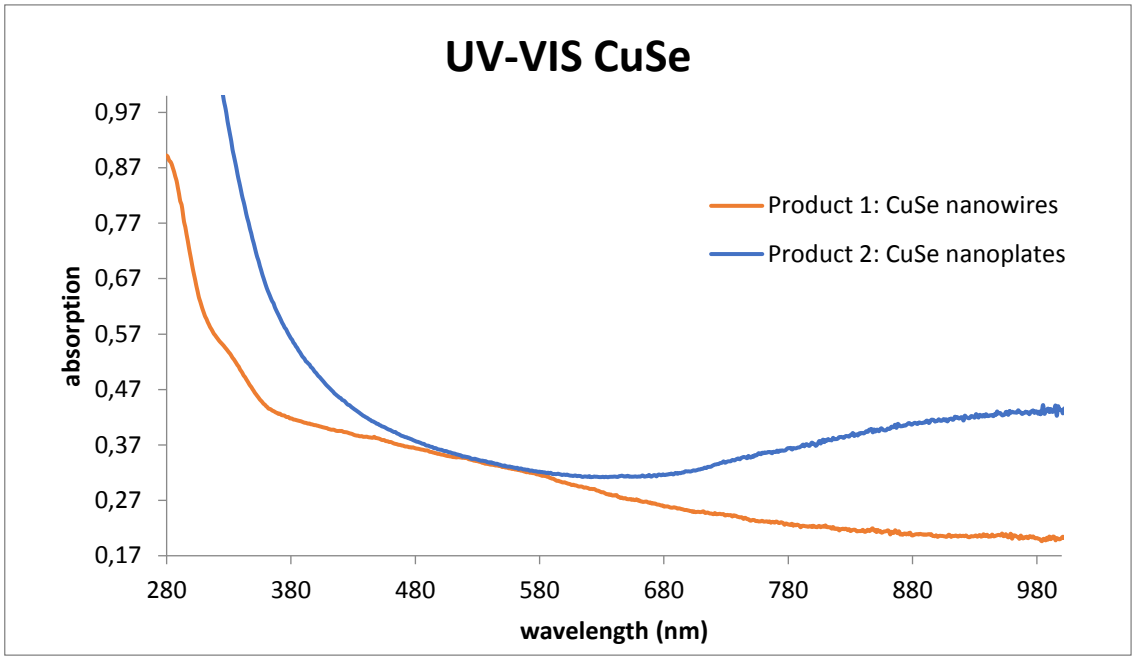

Figure 16: UV-VIS $Cu_{2-x}Se$

As shown in table 3 the ATR-IR measurements between 250 – 4000 nm of the two products. Again, really similar results are shown, because of the oleylamine peaks. These peaks give a definite proof that the oleylamine is still on the surface of the plates and wires.

Table 3: ATR-FTIR $Cu_{2-x}Se$

Vibrational modes	Frequency (cm^{-1}) **Procut 1**	Frequency (cm^{-1}) **Product 2**
ν_{as}(NH_2) and $\nu_s(NH_2)$	around 3300	
δ(=C–H)	3003-3006	
ν_{as}(CH_2) and $\nu s(CH_2)$	2921, 2852	2921, 2852
δ(-C=C)	1694-1688	1690
$\delta(NH_2)$	1583	1585
$\delta(CH_3)$	1456	1466
δ(C-N)	963	966
δ (C-C)		750

ν_s = symmetric stretching vibration; ν_{as} = asymmetric stretching vibration; δ = bending vibration

Figure 17 shows the XRD of product 2, the $Cu_{2-x}Se$ nanoplates.

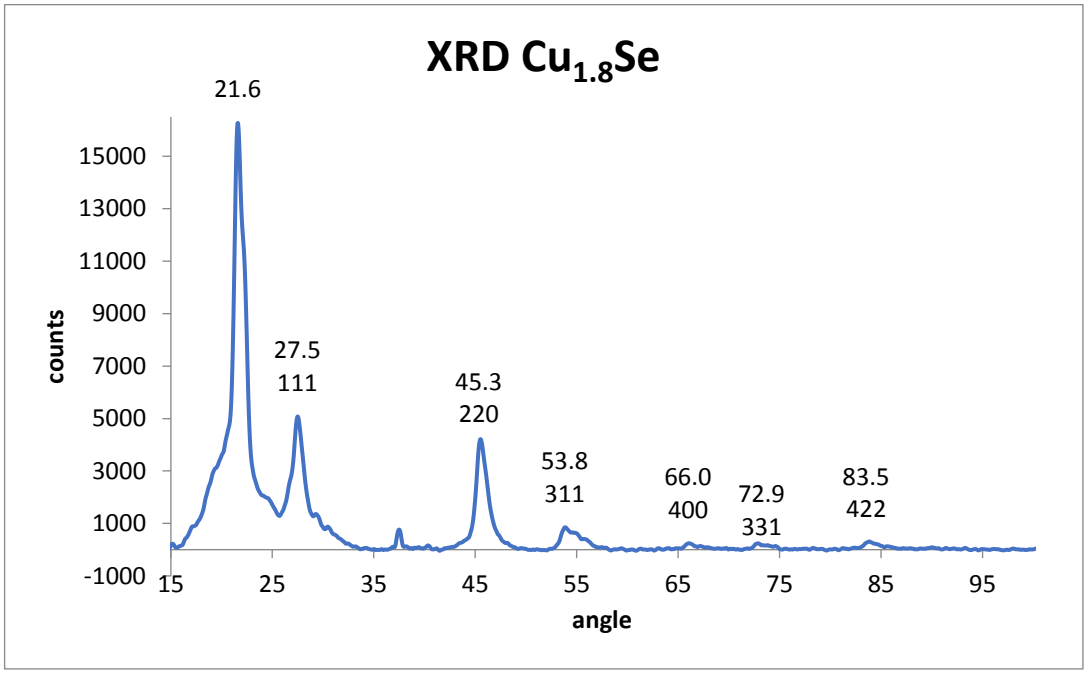

Figure 17: XRD $Cu_{1.8}Se$

The spectrum was compared to the file number 01-088-2045, a face centered cubic CuSe structure. The diffraction point at the angle of 27.5 (111) accordant to the compared pattern. The next point at an angle of 45.3 (220) as well as other points at angles of 53.8 (311), 66.0 (400), 72.9 (331), and 83.5 (422). Resulting that the pattern of product 2 shows clearly the $Cu_{1.8}Se$ face centered cubic (fcc).

Product 1, the nanowires are very difficult to reproduce. It was washed four times before it was cleaned of impurities. Unfortunately, it was not possible to reproduce the same nanowires again.

3.3 Iron sulphide (FeS)

Iron sulphide was produced either with iron(III)trichloride hexahydrate ($Fe[III]Cl_3*6H_2O$) to get product 1, shown in figure 18 or with iron(II)dichloride tetrahydrate ($Fe[II]Cl_2*4H_2O$) to get product 2, which is shown in figure 19. Whichever iron metal salt was used, it was dissolved in NMP beforehand and added via 'hot injection' into the stirring oleylamine-sulphide mix. Sulphur was reduced beforehand with oleylamine the same way as the CuS nanoplates. Temperatures from 150°C until 210°C were tried out and the time was changed from one to two hours. Product 1, which was synthesised with $Fe[III]Cl_3*6H_2O$ as educt was made with a concentration ratio of 1:2 mmol (Fe:S) at 210°C and reacted for 1 hour. The result was thin dark brown nanosheets with a lateral length of 266 +/- 118 nm. Product 2 which was synthesised with $Fe[II]Cl_2*4H_2O$ as educt was made with a concentration ratio of 1:3 mmol (Fe:S) with 200°C and reacted for 1 hour. The thin dark brown nanosheets are smaller and have a lateral length of 212 +/- 73 nm.

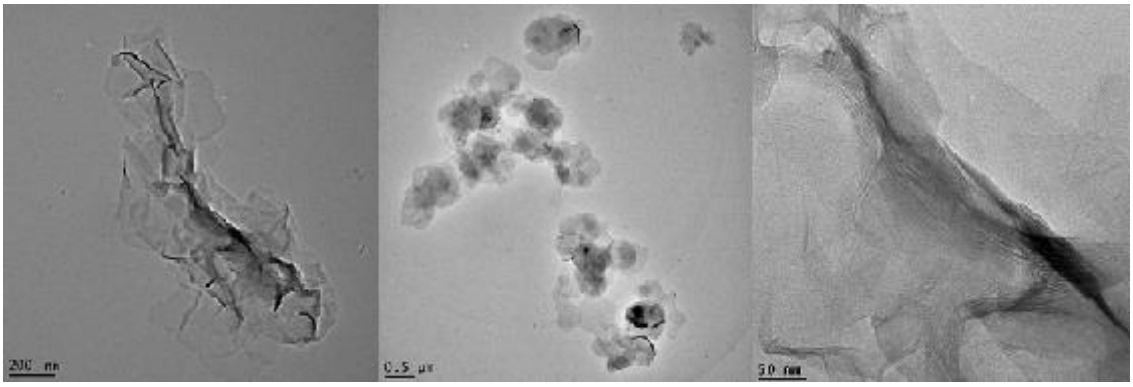

Figure 18: TEM images of FeS nanosheets: product 1 Fe(III)

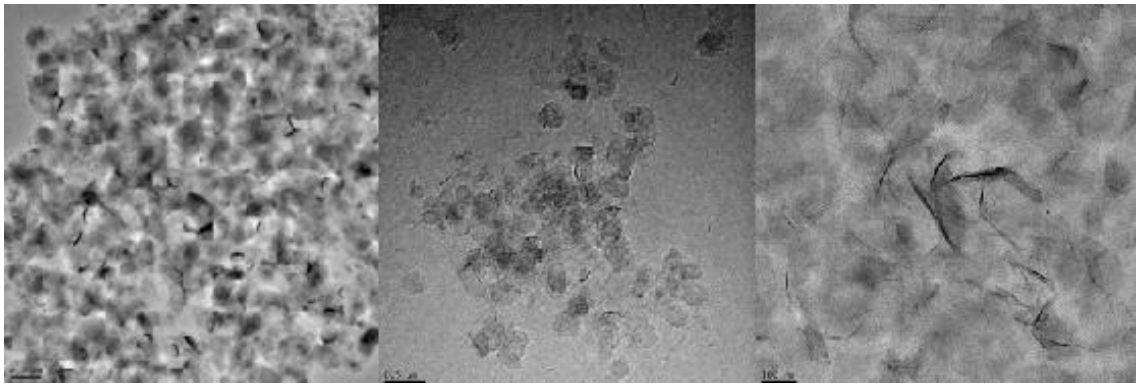

Figure 19: TEM images of FeS nanosheets product 2: Fe(II)

The EDX shows the elemental ratio in product 1 of: Fe: 50% and S: 50% and product 2 has an elemental ratio of Fe: 51% and S: 49%. The peaks match with both spectra as shown in figure 20. The Fe peaks are at: 0.7, 6.4 and 7.1 keV and the sulphide peak is at 2.3 keV. In both spectra there are copper peaks because the sample was plated on a copper TEM grid.

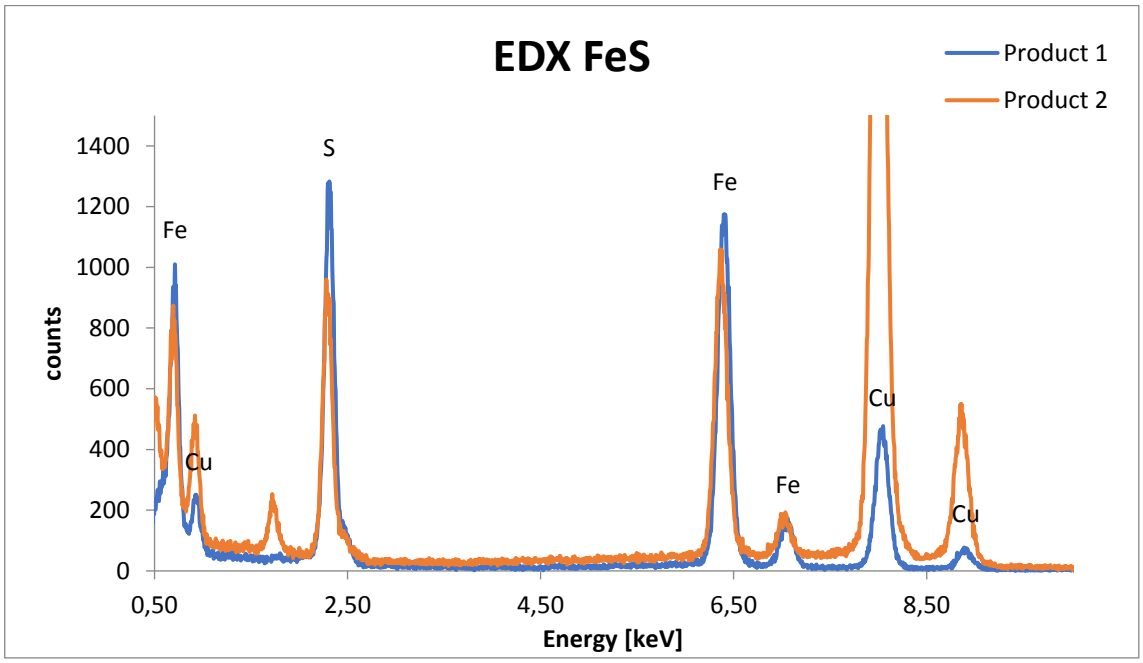

Figure 20: EDX FeS nanosheets

The UV-VIS spectra of FeS nanosheets is shown in figure 21. With product 1 you can clearly see that it has a broad shoulder starting at 380 nm which indicates band gap absorption. Compared with product 2 this same band gap absorption shows a much more rising peak starting at a wavelength of 300 nm.

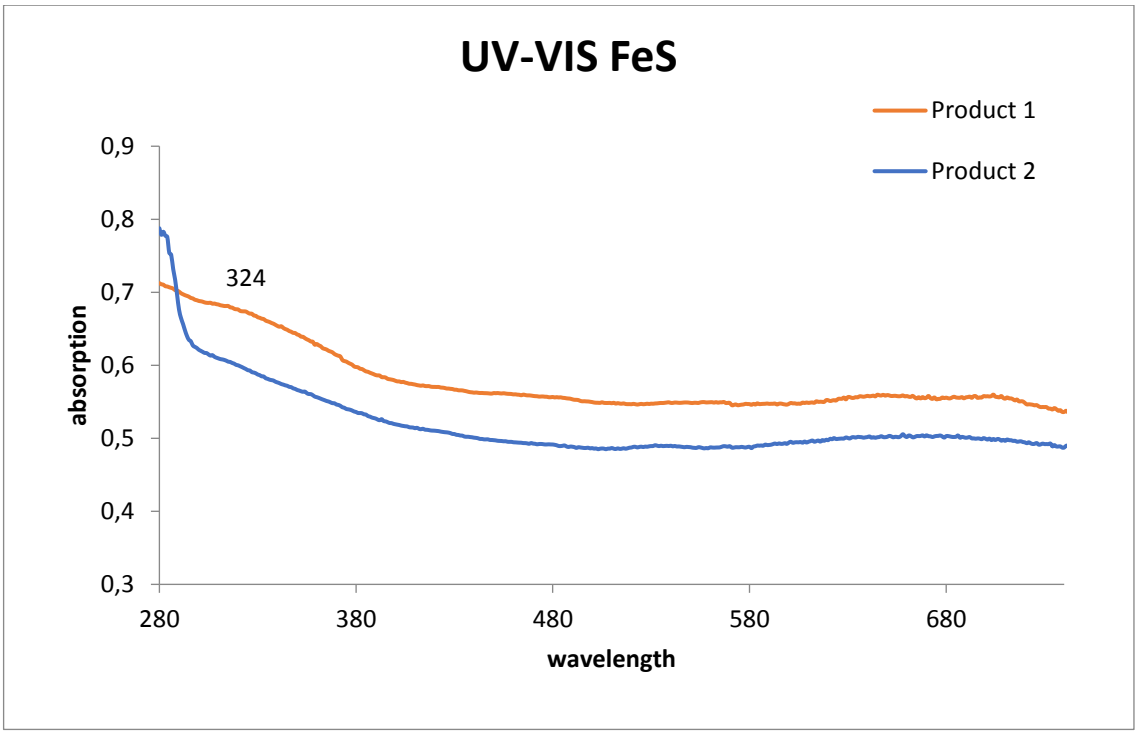

Figure 21: UV-VIS FeS nanosheets

The following table shows the peaks of the ATR-IR measurement of the two FeS nanosheets products clearly arranged. Only product 1 was measured and shows all the typical oleylamine peaks.

Table 4: ATR-FTIR FeS nanosheets

Vibrational modes	Frequency (cm^{-1}) **Procut 1**
v_{as}(NH_2) and v_s(NH_2)	around 3667
v_{as}(CH_2) and vs(CH_2)	2924, 2854
δ(-C=C)	1688
δ(NH_2)	1500
δ(CH_3)	1457
δ(C-N)	967
δ (C-C)	

v_s = symmetric stretching vibration; v_{as} = asymmetric stretching vibration; δ = bending vibration

And as mentioned before a lot of other conditions were tried out. Such as lowering the temperature and increasing the reaction time to 2 hours. But the result was only mixed products.

3.4 Iron selenide ($FeSe_2$)

Iron selenide was produced with iron(II)dichloride tetrahydrate ($Fe[II]Cl_2*4H_2O$), which is shown in figure 22. The iron metal salt was again dissolved in NMP beforehand and added via 'hot injection' into the stirring oleylamine-selenide mix. Selenium was reduced beforehand with oleylamine the same way as the $Cu_{1.8}Se$ nanoplates. The product was synthesised with a concentration ratio of 1:3 mmol (Fe:Se) at 160°C and reacted for 30 minutes. The result was similar to FeS, thin black nanosheets with a lateral length of a micron to sub-micron range. Because of the drying effect the nanosheets curl and the density increases which is shown in the TEM images. [12]

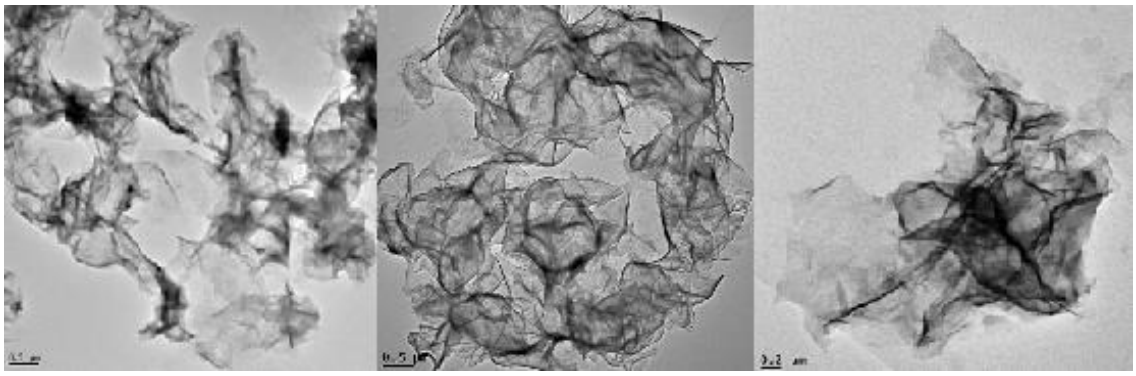

Figure 22: TEM images of iron selenide nanosheets

EDX gives an elemental ratio of Fe(II): 43% and Se: 57% and shows iron peaks at: 0.7, 6.4 and 7 keV and selenide peaks at: 1.4, 11.2 and 12.3 keV.

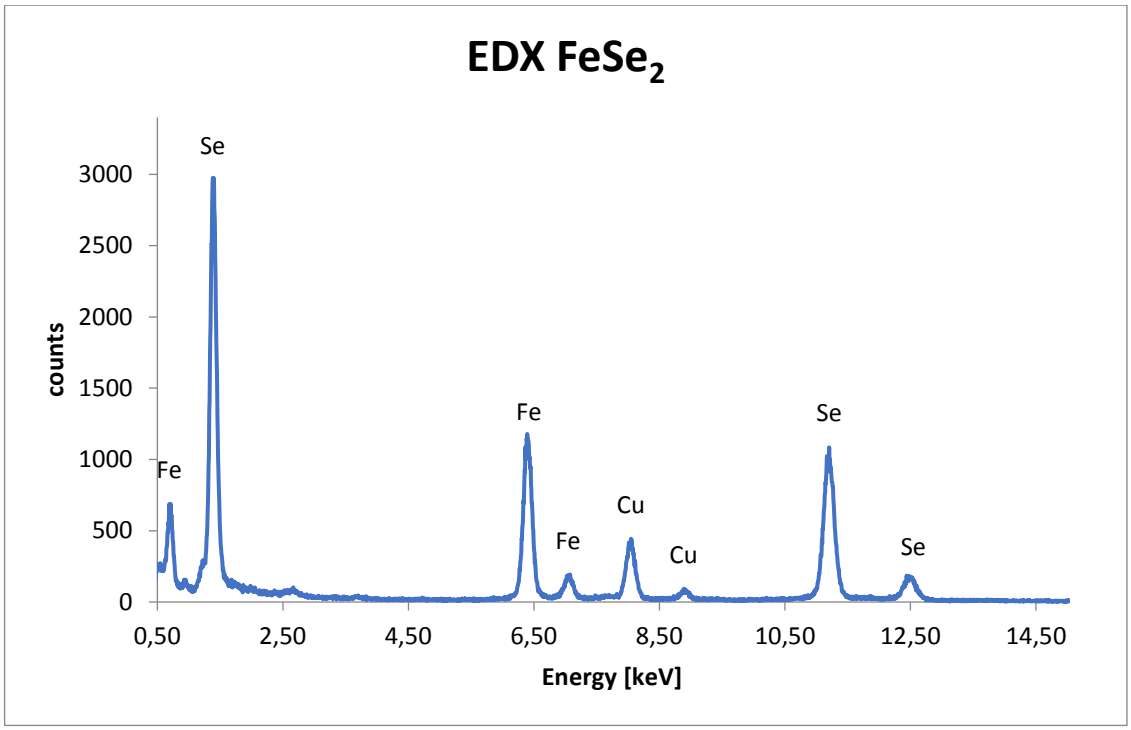

Figure 23: EDX of $FeSe_2$ nanosheets

The UV Vis shows an increasing shoulder peak starting at 430nm which could indicate band gap absorption.

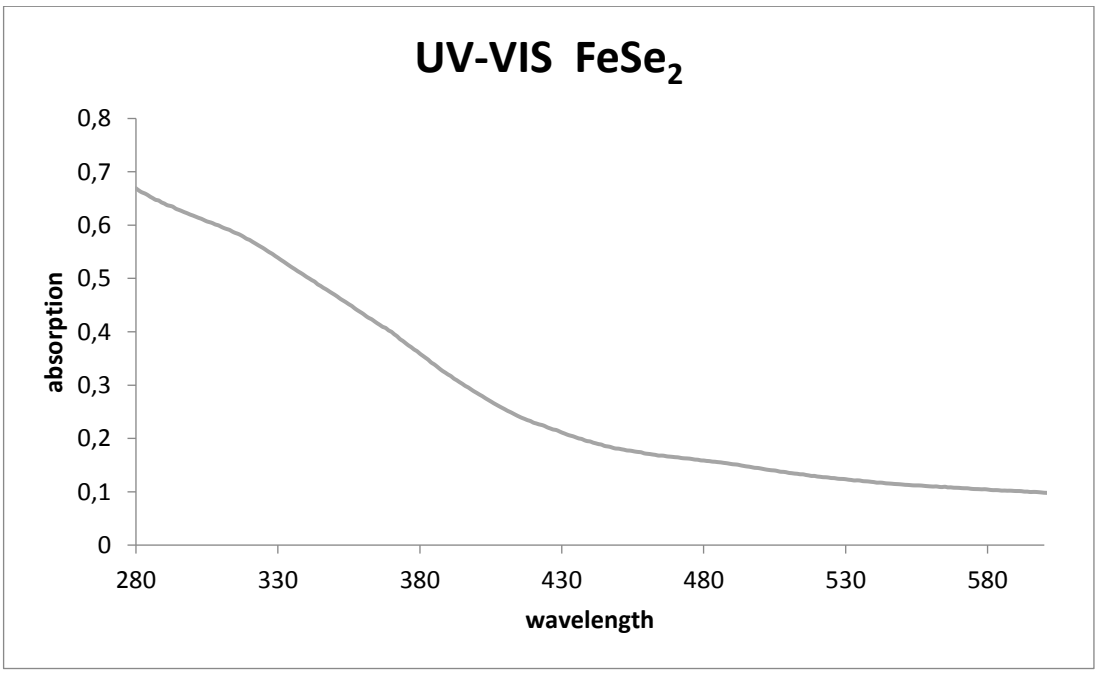

Figure 24: UV-VIS $FeSe_2$ nanosheets

The ATR FTIR only shows peaks of bending vibrations of NH_2, CH_3, C-N and C-C.

Table 5: ATR-FTIR of $FeSe_2$ nanosheets

Vibrational modes	Frequency (cm^{-1}) **$FeSe_2$ nanosheets**
δ(NH_2)	1500
δ(CH_3)	1466
δ(C-N)	967
δ (C-C)	750

v_s = symmetric stretching vibration; v_{as} = asymmetric stretching vibration; δ = bending vibration

The XRD measurement shows a $FeSe_2$ orthorhombic pattern and was taken from the paper: *Adaptable surfactant-mediated method for the preparation of anisotropic metal chalcogenide nanomaterials*. [12]

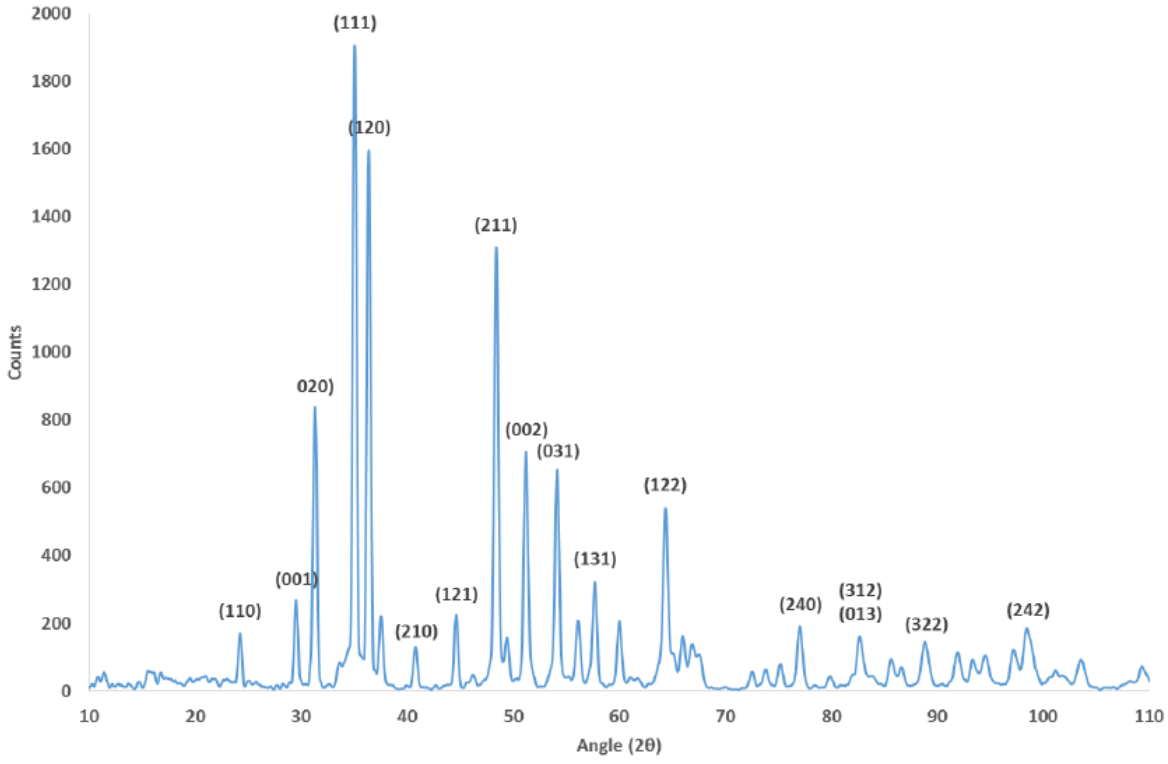

Figure 25: XRD $FeSe_2$ nanosheets taken from [12]

A lot of experiments were also carried out with Fe[III]Cl_3*6H_2O salt as an educt, but they only led to impurities. As first thought small particles were produced as shown in the TEM images in figure 26 but they turned out to be unreacted iron that reacted to brown iron oxide particles as a side product.

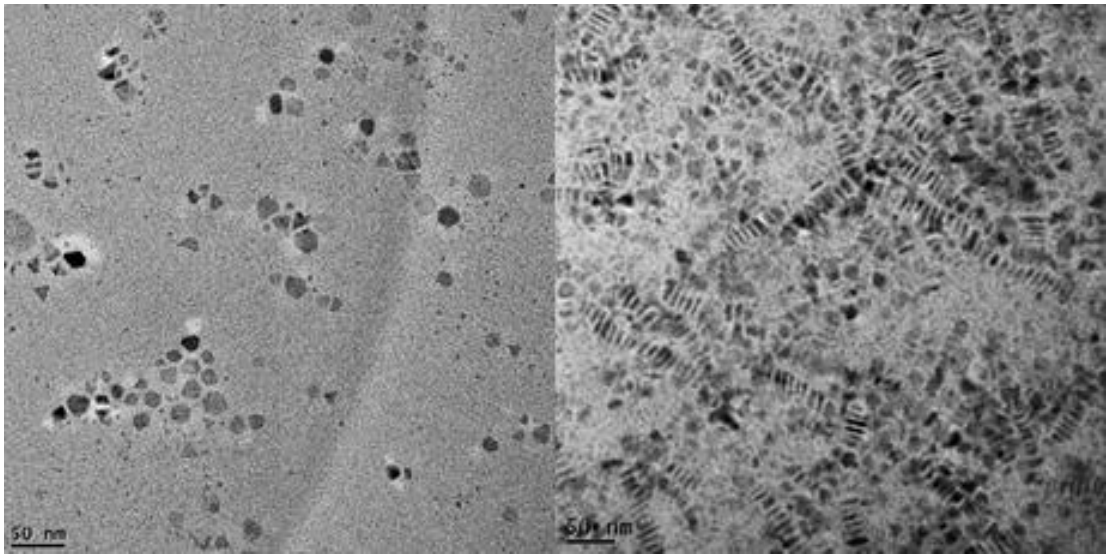

Figure 26: TEM images of iron-oxide impurities

3.8 Nickel selenide (NiSe)

To produce the nickel selenide nanoscrolls, as shown in figure 27, nickeldichloride hexahydrate ($Ni(II)Cl_2*6H_2O$) was used as a metal salt. It was dissolved in NMP and added via 'hot injection' to a stirring selenium-oleylamine mix. Selenium was reduced beforehand like explained before with oleylamine. The conditions were 170°C, 30 minutes and a concentration ratio of 1:2 mmol (Ni:Se). The lateral length of the black nanoscrolls is 69 +/-25 nm.

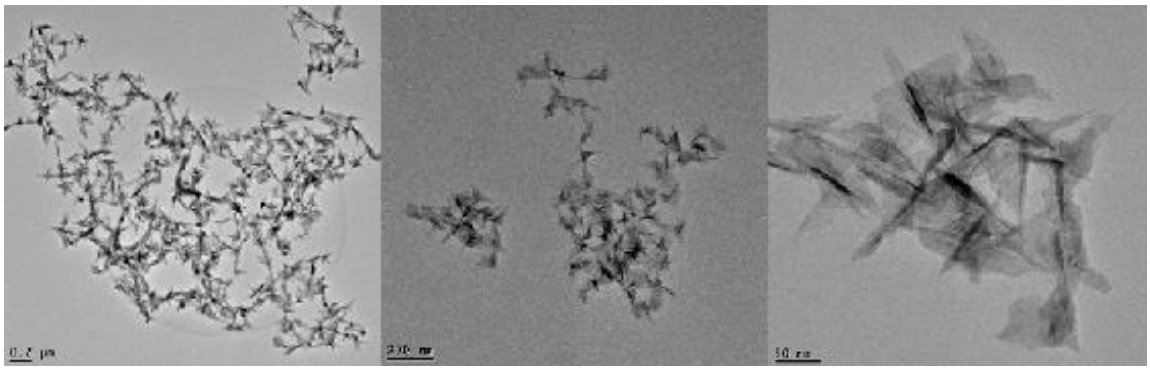

Figure 27: TEM picture of NiSe nanoscrolls

EDX showed an elemental ratio of Ni 42% and Se: 58%.and nickel peaks at 0.85 and 7.44 keV and selenide peaks at 1.4, 11.2 and 12.5 keV as shown in figure 28.

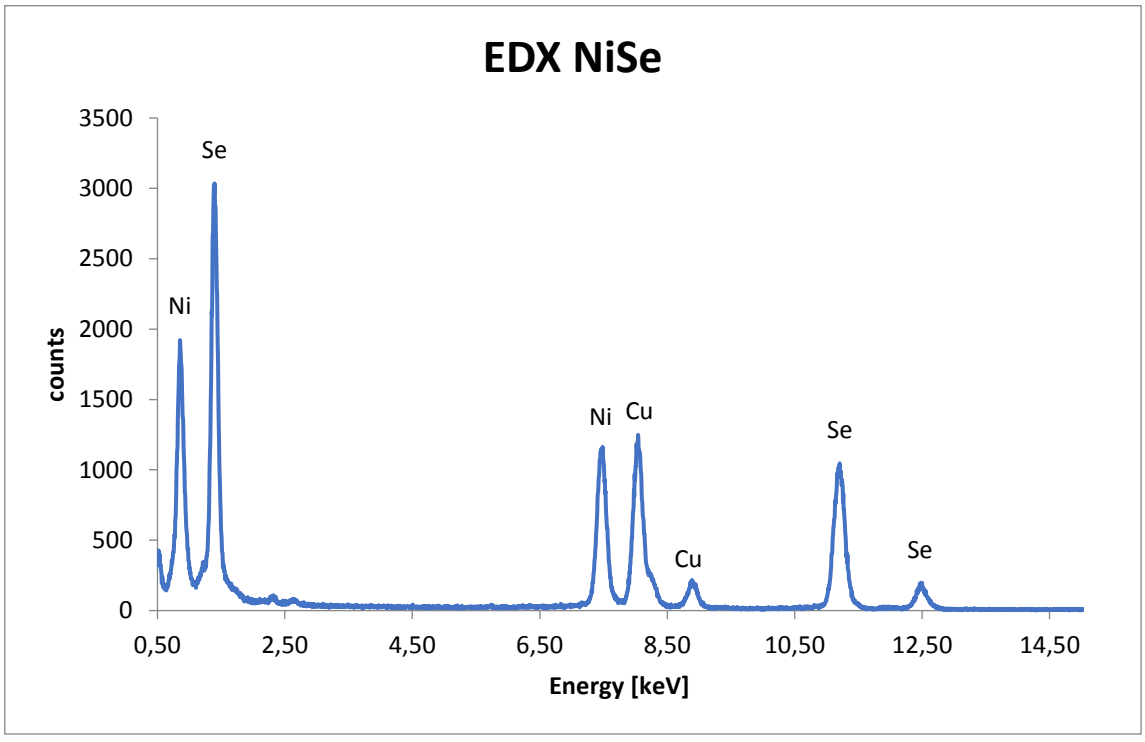

Figure 28: EDX NiSe nanoscrolls

In the UV VIS range of 280-600nm no optical properties could be measured as shown in figure 29.

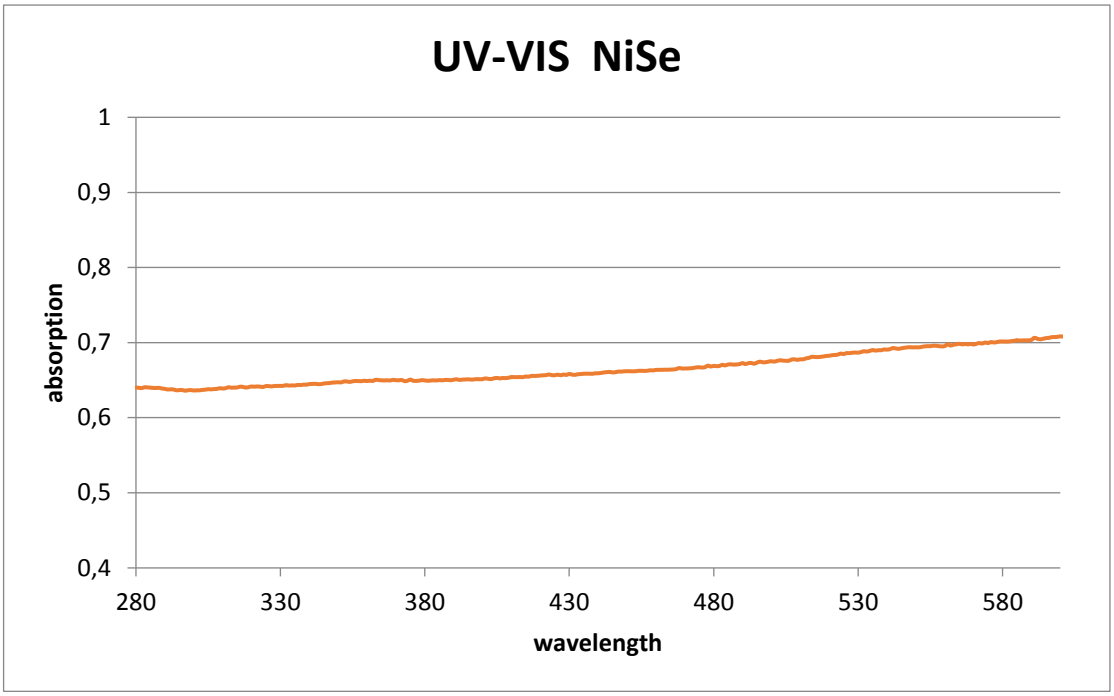

Figure 29: UV-VIS NiSe

The ATR FTIR shows peaks of bending vibrations of -C=C; NH_2, CH_3, C-N and C-C.

Table 6: ATR FTIR NiSe nanoscrolls

Vibrational modes	Frequency (cm^{-1}) **NiSe nanoscrolls**
δ(-C=C)	1689
δ(NH_2)	1500
δ(CH_3)	1460
δ(C-N)	966

4. Experimental

4.1 Synthesis of copper sulphide (CuS)

copper (II) chloride dehydrate: ($CuCl_2$*2H_2O; 1mmol, 0.174g, M: 174 g/mol, blue powder)
sulphur: (S, 2 or 3mmol; 0.064g or 0.096g, M: 32 g/mol, yellow plates)

In a 100ml round bottom flask oleylamine (50ml) was degassed under vacuum at 80°C and afterwards covered with argon. Sulphur was added as solid and the temperature was raised to the temperature (120°C -180°C). The yellow mix turned orange and with higher temperatures red. Afterwards copper (II) chloride dehydrate in N-methyl-2-pyrrolidon (NMP) (5ml) was added with a syringe quickly and the red solution became dark green/brown. The reaction mix stirred for 30 minutes. The reaction was stopped by cooling it down with tap water and methanol (50ml) was added. The mix was divided into four sample tubes and placed in the freezer for 10 minutes. Subsequently the four samples were centrifuged (9000rpm, 10min). The product was redispersed in chloroform and afterwards stored in the freezer.

Colour of particles: dark green

4.2 Synthesis of copper selenide ($Cu_{2-x}Se$)

copper (II) chloride dehydrate: ($CuCl_2$*2H_2O; 1mmol, 0.174g, M: 174 g/mol, blue powder)
selenium: (Se, 2mmol, 0.158g, M: 79 g/mol, dark grey powder)

Oleylamine (50ml) was degassed under vacuum in a 100ml round bottom flask at 80°C and afterwards flushed with argon. Selenium was added as solid to the solution and the temperature was raised to 190°C. The mix turned grey, the higher the temperature got and the more selenium was dissolved the solution turned more and more orange. The alloy stirred overnight.
On the next day when all of the selenium was fully dissolved the temperature was lowered down/raised to the particular temperature (150°C – 220°C) again. As soon as the temperature was reached copper (II) chloride dehydrate in NMP (5ml) was added quickly by syringe. The orange solution turned dark brown/ green and the mix reacted for a certain time (30min – 3h). Afterwards the reaction was cooled down with tap water and methanol (50ml) was added. The samples were put in the freezer for 10 minutes

and then centrifuged (9000rpm, 10min). The product was redispersed in chloroform and stored in the freezer.

Colour of particles: black

4.3 Synthesis of iron suphide (FeS)

iron(III) chloride hexahydrate: ($Fe(III)Cl_3*6H_2O$, 1mmol, 0.27g, M: 270 g/mol, orange/brown powder)

sulphur: (S, 2 mmol; 0.064g, M: 32 g/mol, yellow plates)

The experiment was started by degassing oleylamine (50ml) under vacuum at 80°C in a flask and covering it afterwards with argon. Sulphur was added as solid and the temperature was raised (150°C – 210°C). The solution became red/orange. After all the sulphur was fully dissolved iron(III) chloride hexahydrate was added in NMP (5ml). The solution became black/violet and stirred for a certain time (1h – 2h). Again the reaction was stopped by cooling it down with tap water and adding methanol (50ml). The alloy was divided into four samples, placed in the freezer for 10 minutes and afterwards centrifuged (9000rpm, 10min). The product was redispersed in chloroform and then stored in the freezer.

Colour of particles: dark brown

4.4 Synthesis of iron sulphide (FeS)

iron(II) chloride tetrahydrate: ($Fe(II)Cl_2*4H_2O$, 1mmol, 0198g, M: 198 g/mol, orange powder)

sulphur: (S, 2 mmol; 0.064g, M: 32 g/mol, yellow plates)

First of all oleylamine (50ml) was degassed under vacuum at 80°C in a flask and flushed afterwards with argon. Sulphur was added as solid and the temperature was raised (200°C – 220°C). The solution became red and after all the sulphur was fully dissolved iron(II) chloride tetrahydrate was added in NMP (5ml). The solution turned immideately black and stirred for a certain time (30min – 2h). Afterwards the reaction was stopped by cooling it down with tap water and adding methanol (50ml). The alloy was divided into four samples, placed in the freezer for 10 minutes and afterwards centrifuged (9000rpm, 10min). The product was redispersed in chloroform and then stored in the freezer.

Colour of particles: dark brown

4.5 Synthesis of iron selenide ($FeSe_2$)

iron(III) chloride hexahydrate: ($Fe(III)Cl_3*6H_2O$, 1mmol, 0.27g, M: 270 g/mol, orange/brown powder)

selenium: (Se, 2mmol, 0.158g, M: 79g/mol, dark grey powder)

To start the experiment oleylamine (50ml) was degassed under vacuum at 80°C and covered with argon afterwards. Then selenium was added as solid and the temperature was raised to 190°C. The first yellow mix got after adding the selenium grey and with higher temperature more and more orange. The mix stirred overnight.
On the next day the temperature was lowered to a certain temperature (160°C – 180°C) and as soon as the selenium was fully dissolved iron(III) chloride hexahydrate in NMP (5 ml) was added via syringe. The mix stirred for a certain time (30min – 3h) and the orange solution got dark brown. Afterwards the reaction was stopped by cooling it down under tap and adding methanol (50ml). The alloy was divided into four sample tubes and put in the freezer for 10 minutes and then centrifuged (10min; 9000rpm). The product was redispersed in chloroform and stored in the freezer.

Colour of particles: black

4.6 Synthesis of iron selenide ($FeSe_2$)

iron(II) chloride tetrahydrate: ($Fe(II)Cl_2*4H_2O$, 1mmol, 0.198g, M: 198 g/mol, orange powder)

selenium: (Se, 2mmol or 3mmol, 158mg or 0,237g, M: 79g/mol, dark grey powder)

Under vacuum at 80°C oleylamine (50ml) was degassed in a round bottom flask (100ml). Afterwards it was covered with argon and selenium was added as solid. The yellow solution turned grey, black and the temperature was raised to 190°C. When the temperature of 190°C was reached the mix got orange/red and stirred overnight.
On the next day the temperature was lowered to 160°C as soon as the selenium was fully dissolved. iron(II) chloride tetrahydrate in NMP (5ml) was added via syringe rapidly. The dark orange solution turned immediately black. The mixture stirred for a certain time (30 min – 2h) at 160°C. The reaction was stopped by cooling it down under tap water and adding methanol (50ml). The brown mix was placed in the freezer for 10 minutes. Afterwards the divided samples were centrifuged to isolate the particles (10Min, 9000rpm). The product was redispersed in chloroform and the product wrapped up in parafilm was stored in the freezer.

Colour of particles black

4.7 Synthesis of nickel selenide (NiSe)

Nickel(II) chloride hexahydrate: ($Ni(II)Cl_2*6H_2O$,1mmol, 0.237g , M: 237.69g/mol, green powder)

selenium: (Se, 2mmol, 158mg, M: 79g/mol, dark grey powder)

At a temperature of 80°C oleylamine (50ml) was degassed under vacuum in a round bottom flask and afterwards flushed with argon.
Sulphur was added as solid and the yellow solution became orange. The temperature was raised to 190°C and the more and more darker becoming mix stirred overnight. On the next day when all selenium was dissolved the temperature was raised/ lowered to a certain amount (160°C - 180°C). Afterwards nickel(II) chloride hexahydrate mixed with NMP (5ml) was added via syringe quickly. The solution turned immediately dark brown/ black and the mix reacted for a certain time(30min – 2h) while stirring. The reaction was stopped by cooling it down under tap water and methanol (50ml) was added. The mix was divided into four samples and placed in the freezer for 10 minutes. To isolate the product the alloy got centrifuged (10min; 9000rpm). The product was redispersed in chloroform and stored in the freezer.

Colour of particles black

5 Summary and Outlook

The aim of this thesis was to produce different metal chalcogenide nanomaterials via hot injection approach. The solvent and reducing agent of the chalcogenide was oleylamine and the metal salt was dissolved before in NMP. With this same approach nine different products, as shown in table 7, were produced with either different materials or kinetic conditions.

Table 7: All products listed

Materials	Form/ Colour	Size	Reaction conditions		
			Temperature	Concentration ratio	Time
CuS	dark green hexagonal nanoplates	535 +/- 119 nm	180°C	1:3 (Cu/S) mmol	30 min
CuS	dark green hexagonal nanoplates	408 +/- 235 nm	160°C	1:2 (Cu/S) mmol	30 min
CuS	dark green hexagonal nanoplates	49 +/- 13 nm	120°C	1:2 (Cu/S) mmol	30 min
$Cu_{2-x}Se$	black nanowires	164 +/- 64 nm	180°C	1:2 (Cu/Se) mmol	30 min
$Cu_{1.8}Se$	black triangular nanoplates	25 +/- 11 nm	210°C	1:2 (Cu/Se) mmol	30 min
FeS	dark brown nanosheets	266 +/- 118 nm	210°C	1:2 (Fe^{III}/S) mmol	1 h
FeS	dark brown nanosheets	212 +/- 73 nm	200°C	1:3 (Fe^{II}/S) mmol	1 h
$FeSe_2$	black nanosheets	sub-micron range	160°C	1:3 (Fe^{II}/Se) mmol	30 min
NiSe	black nanoscrolls	69 +/- 25 nm	170°C	1:2 (Ni/Se) mmol	30 min

Sulphur was always reduced beforehand with degassed oleylamine under inert conditions to sulphide at 80°C, which took an hour. However, selenium reducing to selenide needed much higher reaction temperatures at 220°C and the reaction was mostly done overnight and was done under inert conditions as well. In general reactions with selenide never worked below a temperature of 120°C. The probable reason being that selenide oxidizes back into selenium with lower temperatures.

The products of copper sulphide were hexagonal dark green nanoplates, clearly visible in TEM. The best results were achieved with a reaction time of thirty minutes. The smaller the reaction temperature, the smaller the resulting nanoplates. Additionally, the

concentration ratio was changed from 1:3 (Cu/S) mmol to 1:2 (Cu/S) mmol. The atomic ratio of the two larger products of CuS is: copper: 55 % and sulphide: 45 % and the product with the small nanoplates shows an elemental ratio of: Cu: 52 % and S: 48 %. The optical measurement of the three different CuS products show a broad plasmon absorption towards the IR region and a band gap absorption below 400 nm. The ATR-FTIR measurement shows that oleylamine is still on the surface and the XRD measurement proves that the CuS nanoplates are hexagonal (hex).

Copper selenium reactions resulted into two different products, TEM images were taken from of both. Black $Cu_{2-x}Se$ nanowires and black $Cu_{1.8}Se$ triangular nanoplates. The nanowires were produced under the conditions of 180°C, a reaction time of 30 minutes and a concentration ratio of 1:2 mmol (Cu:Se). The triangular nanoplates were produced with a reaction time of 30 min, 210°C and a concentration ratio of 1:2 mmol (Cu:Se). The elemental ratio of the nanowires is Cu 60 % and Se: 40 % and of the nanoplates is Cu 65 % and Se: 35 %. The nanowires show only a band gap absorption at 280°nm and the nanoplates show a band gap shoulder at 330 nm but also the plasmon absorption at 780 nm. Both products show at the ATR-FTIR measurement oleylamine peaks, however, the $Cu_{2-x}Se$ nanowires were difficult to reproduce that is why only XRD was measured from the triangular nanoplates. The results show clearly the face centered cubic (fcc) pattern of $Cu_{1.8}Se$.

It was very interesting to see, that reactions with iron turned out to be different if the iron(II)-salt or the iron(III)-salt as a precursor was taken. However, both products of FeS were thin dark brown nanosheets, clearly visible in TEM images and their best resulting reaction time was 1 hour for both products. Product 1, which was synthesised with $Fe[III]Cl_3*6H_2O$ as educt was made with a concentration ratio of 1:2 mmol (Fe:S) at 210°C and product 2 which was synthesised with $Fe[II]Cl_2*4H_2O$ as educt was made with a concentration ratio of 1:3 mmol (Fe:S) at 200°C. The EDX shows nearly the same elemental ratio in product 1 of: Fe: 50% and S: 50% and product 2 of Fe: 51% and S: 49%. Optical measurements showed at product 1 a broad shoulder starting at 380 nm which indicates band gap absorption. Compared with product 2 this same band gap absorption shows a much more rising peak starting at a wavelength of 300 nm. The ATR-FTIR measurement was taken from product 1 and shows all the typical oleylamine peaks.

Iron selenide reactions only led to one good product, which was visible in TEM images without impurities. ($Fe[II]Cl_2*4H_2O$) was used as an educt , with a concentration ratio of 1:3 mmol (Fe:Se) at 160°C and reacted for 30 minutes. The result was similar to FeS, thin $FeSe_2$ nanosheets but black in colour with an elemental ratio of Fe: 43% and Se: 57%. Optical measurements show an increasing shoulder peak starting at 430nm which

could indicate band gap absorption and the XRD measurement shows a $FeSe_2$ orthorhombic pattern.

The nickel selenide nanomaterials were produced at 170°C, 30 minutes and a concentration ratio of 1:2 mmol (Ni:Se) resulting in black nanoscrolls, clearly visible in TEM images. The elemental ratio was Ni 42% and Se: 58%, but no optical properties of these nanoscrolls could be measured.

Future work could be done with other metals like cobalt, zinc or indium. Such as the reactions with indium selenide, resulting in small nanoplates which are shown in figure 30. These are preliminary reactions that still have to be optimized.

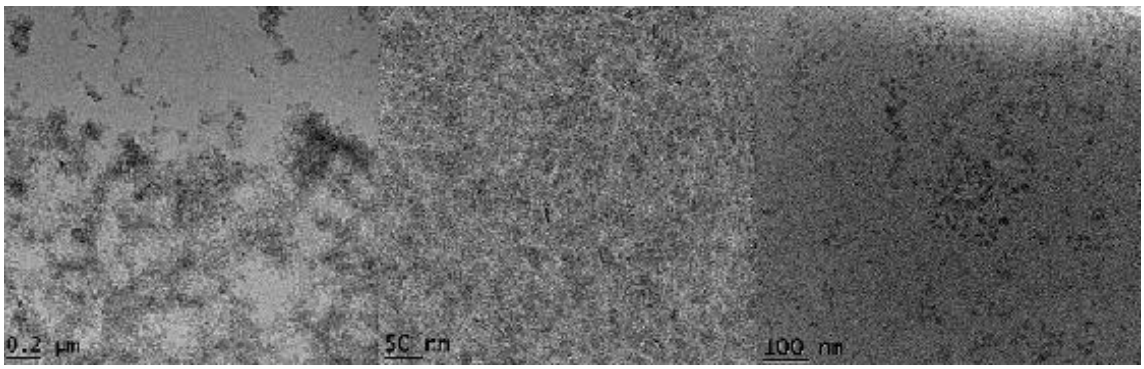

Figure 30: Indium selenide nanoplates

Overall it can be said that a good synthesis strategy to produce two dimensional nanoparticles of different shapes and materials was found.

6 References

[1] X. Zhai, X. Zhang, S. Chen, W. Yang, and Z. Gong, “Oleylamine as solvent and stabilizer to synthesize shape-controlled ZnS nanocrystals with good optical properties,” *Colloids Surfaces A Physicochem. Eng. Asp.*, vol. 409, pp. 126–129, 2012.

[2] “Nano Geschichte: NanoinformationsPortal.” [Online]. Available: https://nanoinformation.at/grundlagen/geschichte-der-nanotechnologie.html. [Accessed: 05-May-2018].

[3] S. Goel, F. Chen, and W. Cai, “Synthesis and biomedical applications of copper sulfide nanoparticles: From sensors to theranostics,” *Small*, vol. 10, no. 4, pp. 631–645, 2014.

[4] S. Mourdikoudis and L. M. Liz-Marzán, “Oleylamine in nanoparticle synthesis,” *Chem. Mater.*, vol. 25, no. 9, pp. 1465–1476, 2013.

[5] P. I. Dolez, *Nanomaterials Definitions, Classifications, and Applications*. 2015.

[6] Y. Li, W. Lu, Q. Huang, C. Li, and W. Chen, “Copper sulfide nanoparticles for photothermal ablation of tumor cells,” *Nanomedicine*, vol. 5, no. 8, pp. 1161–1171, 2010.

[7] “Surface area to volume ratio in nanoparticles | Winner Science.” [Online]. Available: http://winnerscience.com/2012/05/28/surface-area-to-volume-ratio-in-nanoparticles/. [Accessed: 31-May-2018].

[8] “Nanoparticle production - How nanoparticles are made.” [Online]. Available: https://www.nanowerk.com/how_nanoparticles_are_made.php. [Accessed: 07-Jun-2018].

[9] N. H. Ulrich Schubert, *Synthesis of Inorganic Materials*. Weinheim: Wiley-VCH Verlag GmbH, 2000.

[10] I. Khan, K. Saeed, and I. Khan, “Nanoparticles : Properties , applications and toxicities,” *Arab. J. Chem.*, 2017.

[11] F. Asghari, Z. Jahanshiri, M. Imani, M. Shams-Ghahfarokhi, and M. Razzaghi-Abyaneh, *Antifungal nanomaterials: Synthesis, properties, and applications*. Elsevier Inc., 2016.

[12] S. A. McCarthy, R. Ratkic, F. Purcell-Milton, T. S. Perova, and Y. K. Gun'ko, "Adaptable surfactant-mediated method for the preparation of anisotropic metal chalcogenide nanomaterials," *Sci. Rep.*, vol. 8, no. 1, pp. 1–10, 2018.

[13] H. Wei, W. Guo, Y. Sun, Z. Yang, and Y. Zhang, "Hot-injection synthesis and characterization of quaternary Cu2ZnSnSe4nanocrystals," *Mater. Lett.*, vol. 64, no. 13, pp. 1424–1426, 2010.

[14] R. Alsfasser, *Moderne anorganische Chemie: mit CD-ROM*. Berlin, New York: Walter de Gruyters, 2007.

[15] K. J. Klabunde, *Nanoscale Materials in Chemistry*. Weinheim: Wiley, 2001.

[16] J. N. Tiwari, R. N. Tiwari, and K. S. Kim, "Zero-dimensional, one-dimensional, two-dimensional and three-dimensional nanostructured materials for advanced electrochemical energy devices," *Prog. Mater. Sci.*, vol. 57, no. 4, pp. 724–803, 2012.

[17] G. Amin, *ZnO and CuO Nanostructures : Low Temperature Growth , Characterization , their Optoelectronic and Sensing Applications Linköping Studies in Science and Technology ZnO and CuO Nanostructures : Low Temperature Growth , Characterization , their Optoelectroni*, no. April. 2015.

[18] "quantum dot (CHEBI:50853)." [Online]. Available: http://www.ebi.ac.uk/chebi/searchId.do?chebiId=50853. [Accessed: 13-Jun-2018].

[19] C. Edtmaier, "Vo technologie nanostrukturierter materialien," 2017.

[20] Y. J. Zeng, S. S. Lin, A. Volodin, Y. F. Lu, Z. Z. Ye, and C. Van Haesendonck, "Zero-dimensional field emitter based on ZnO quantum dots," *Appl. Phys. Lett.*, vol. 97, no. 14, pp. 95–98, 2010.

[21] "Nanotechnology Introduction - two-dimensional nanomaterials." [Online]. Available: https://www.nanowerk.com/nanotechnology/introduction/introduction_to_nanotechnology_7.php. [Accessed: 07-Jun-2018].

[22] X. Xie *et al.*, "Controlled Fabrication of High-Quality Carbon Nanoscrolls from Monolayer Graphene," *Nano Lett.*, vol. 9, no. 7, pp. 2565–2570, Jul. 2009.

[23] B. Jayasena, S. Subbiah, and C. D. Reddy, "Formation of Carbon Nanoscrolls During Wedge-Based Mechanical Exfoliation of HOPG," *J. Micro Nano-Manufacturing*, vol. 2, no. 1, p. 011003, Jan. 2014.

[24] A. K. Geim *et al.*, “Graphene: status and prospects.,” *Science*, vol. 324, no. 5934, pp. 1530–4, Jun. 2009.

[25] N. Iqbal, I. Khan, Z. H. Yamani, and A. Qurashi, “Sonochemical Assisted Solvothermal Synthesis of Gallium Oxynitride Nanosheets and their Solar-Driven Photoelectrochemical Water-Splitting Applications,” *Sci. Rep.*, vol. 6, no. 1, p. 32319, Oct. 2016.

[26] A. Grigat, F. Lang, and B.-M. Wilke, “"Nanomaterialien" in: Bodengefährdende Stoffe: Bewertung - Stoffdaten - Ökotoxikologie - Sanierung.”

[27] A. Halder, P. Kundu, B. Viswanath, and N. Ravishankar, “Symmetry and shape issues in nanostructure growth,” *J. Mater. Chem.*, vol. 20, no. 23, p. 4763, 2010.

[28] X. Zhao, Z. Bao, C. Sun, and D. Xue, “Polymorphology formation of Cu2O: A microscopic understanding of single crystal growth from both thermodynamic and kinetic models,” *J. Cryst. Growth*, vol. 311, no. 3, pp. 711–715, 2009.

[29] “Unit 1.3 - Definition of Crystals and Anisotropy - YouTube.” [Online]. Available: https://www.youtube.com/watch?v=Iky6-Iqab4c. [Accessed: 11-Jun-2018].

[30] B. Viswanath, P. Kundu, and N. Ravishankar, “Formation of two-dimensional structures by tuning the driving force of chemical reactions: An interpretation of kinetic control,” *J. Colloid Interface Sci.*, vol. 330, no. 1, pp. 211–219, 2009.

[31] Anthony R. West, *Solid State Chemistry and its Applications*. Chichester, West Sussex: John Wiley & Sons, Ltd, 2014.

[32] J. . Venables, “The electron microscopy of deformation twinning,” *J. Phys. Chem. Solids*, vol. 25, no. 7, pp. 685–692, Jul. 1964.

[33] Y. H. Zhao, X. Z. Liao, Y. T. Zhu, Z. Horita, and T. G. Langdon, “Influence of stacking fault energy on nanostructure formation under high pressure torsion,” *Mater. Sci. Eng. A*, vol. 410–411, pp. 188–193, 2005.

[34] “Twinning - Chemistry LibreTexts.” [Online]. Available: https://chem.libretexts.org/Core/Inorganic_Chemistry/Crystallography/Twinning. [Accessed: 18-Jun-2018].

[35] “Twins – Chemical Crystallography.” [Online]. Available: http://www.xtl.ox.ac.uk/resources/twin.html#2. [Accessed: 18-Jun-2018].

[36] “What is Melting Point? - Definition, Range & Determination - Video & Lesson Transcript | Study.com.” [Online]. Available: https://study.com/academy/lesson/what-is-melting-point-definition-range-determination.html. [Accessed: 16-Jun-2018].

[37] S. Bhatt, R. Kumar, and M. Kumar, “Specific heat and thermal conductivity of nanomaterials,” *Mod. Phys. Lett. B*, vol. 31, no. 02, p. 1750011, Jan. 2017.

[38] Gutmann / Hengge, *Anorganische Chemie Eine Einführung*. 1990.

[39] W. Holleman, *Lehrbuch der Anorganischen Chemie*. München: Walter de Gruyter, 2007.

[40] “(98) Professor Hao Zeng - Waterloo Institute for Nanotechnology (WIN) Seminar - YouTube.” [Online]. Available: https://www.youtube.com/watch?v=8QO18Xj-nxQ. [Accessed: 08-Jun-2018].

[41] S. C. Riha, D. C. Johnson, and A. L. Prieto, “Cu 2Se nanoparticles with tunable electronic properties due to a controlled solid-state phase transition driven by copper oxidation and cationic conduction,” *J. Am. Chem. Soc.*, vol. 133, no. 5, pp. 1383–1390, 2011.

[42] W. Wang, S. Y. Wang, K. Y. Wang, Y. L. Gao, and M. Liu, “A facile route to FeS nanowires via an infiltration process,” *Solid State Commun.*, vol. 140, no. 7–8, pp. 325–328, 2006.

[43] M. Wu *et al.*, “A low band gap iron sulfide hybrid semiconductor with unique 2D [Fe 16S20]8- layer and reduced thermal conductivity,” *Chem. Commun.*, vol. 46, no. 10, pp. 1649–1651, 2010.

[44] K. D. Oyler, X. Ke, I. T. Sines, P. Schiffer, and R. E. Schaak, “Chemical synthesis of two-dimensional iron chalcogenide nanosheets: FeSe, FeTe, Fe(Se,Te), and FeTe2,” *Chem. Mater.*, vol. 21, no. 15, pp. 3655–3661, 2009.

[45] F.-C. Hsu *et al.*, “Superconductivity in the PbO-type structure -FeSe,” *Proc. Natl. Acad. Sci.*, vol. 105, no. 38, pp. 14262–14264, Sep. 2008.

[46] A. K. Dutta *et al.*, “Synthesis of FeS and FeSe nanoparticles from a single source precursor: A study of their photocatalytic activity, peroxidase-like behavior, and electrochemical sensing of H2O2,” *ACS Appl. Mater. Interfaces*, vol. 4, no. 4, pp. 1919–1927, 2012.

[47] P. A. Nwofe, R. A. Chikwen, P. E. Agbo, and H. U. Igwe, “Deposition and Characterization of Nickel Selenide Thin Films for Applications in Optoelectronic Devices,” *Asian J. Sci. Res.*, vol. 10, no. 1, pp. 43–49, Dec. 2016.

[48] D. Mijatovic, J. C. T. Eijkel, and A. van den Berg, “Technologies for nanofluidic systems: top-down vs. bottom-up—a review,” *Lab Chip*, vol. 5, no. 5, p. 492, Apr. 2005.

[49] L. Wu, A. Mendoza-Garcia, Q. Li, and S. Sun, “Organic Phase Syntheses of Magnetic Nanoparticles and Their Applications,” *Chem. Rev.*, vol. 116, no. 18, pp. 10473–10512, 2016.

[50] C. De Mello Donegá, P. Liljeroth, and D. Vanmaekelbergh, “Physicochemical evaluation of the hot-injection method, a synthesis route for monodisperse nanocrystals,” *Small*, vol. 1, no. 12, pp. 1152–1162, 2005.

[51] “Oleylamine technical grade, 70% | Sigma-Aldrich.” [Online]. Available: https://www.sigmaaldrich.com/catalog/product/aldrich/o7805?lang=de&region=AT. [Accessed: 08-Jun-2018].

7 Chemicals and Equipment

All chemicals for the synthesis of monomers, precursors or substrates were purchased from commercial sources (Sigma Aldrich, Fluka, Alfa Aesar). These were used without further purification.

For TEM analysis, the materials were dispersed at approximately 0.1 $mgmL^{-1}$ in hexane or chloroform by sonication for ~5 min in a sonic bath. They were then deposited on a 300 mesh thin carbon or holey thin carbon coated copper or molybdenum grids using a 1.5 µl aliquot of this dispersion. Copper containing samples were instead deposited on Mo grids, with the same coating, in order to measure elemental ratio by EDX. Measurements were performed using a Fei Titan microscope at an accelerating voltage of 400 kV, using bright field imaging. Size measurement were calculated from >100 measurements in the resulting images using ImageJ.

XRD was performed using a PANalytical X'Pert Powder diffractometer. The sample was prepared from a saturated solution in hexane or chloroform, then deposited onto a glass slide by pipette, with drying then additional depositions to build a dense layer of material with good adhesion to the glass. The XRD was measured over 3–6 hours for angles 10–155 (2θ). Baseline correction and smoothing were also performed.

ATR FTIR spectroscopy was performed using a Perkin Elmer Spectrum One NTS FTIR spectrometer. The liquid samples were deposited directly onto the diamond crystal. No further pressure was applied for crystal contact. ATR sampling was then performed over 10 min between 350–4000 cm−1. Baseline correction and smoothing were also performed.

UV-IR absorption measurements were performed using a Perkin Elmer Lambda1050 spectrometer. Samples were prepared by dispersion in hexane or chloroform and measurements were run over 250–2500 nm, at 2 nm intervals. In some cases smoothing was performed.

8 List of Figures

9 List of Shemes

10 List of Tables

11 Appendix

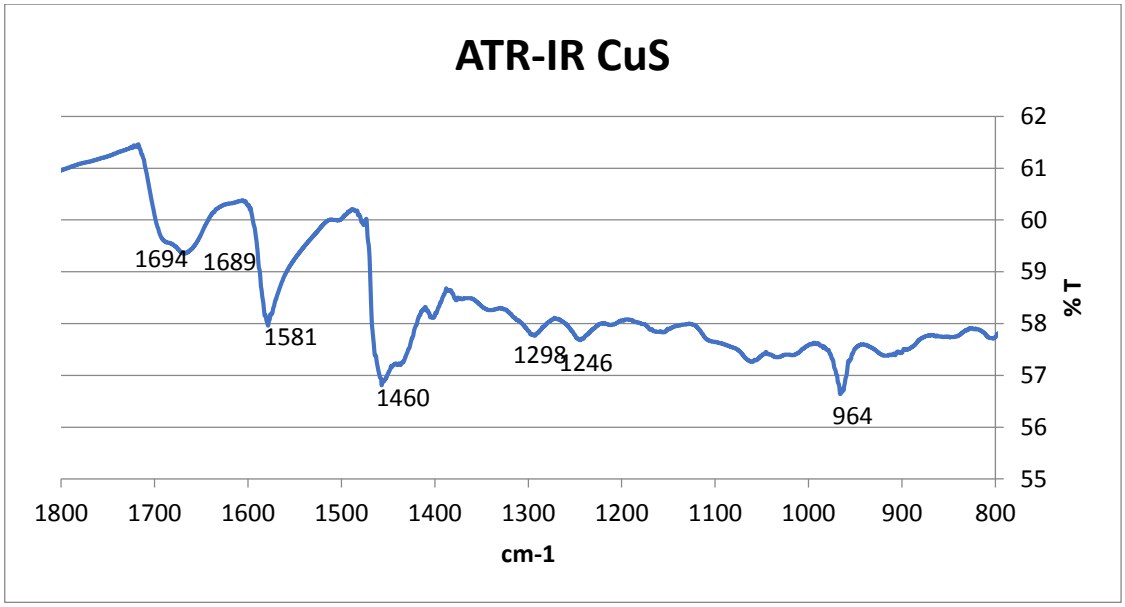

Figure 31: ATR-FTIR CuS nanoplates (product 1)

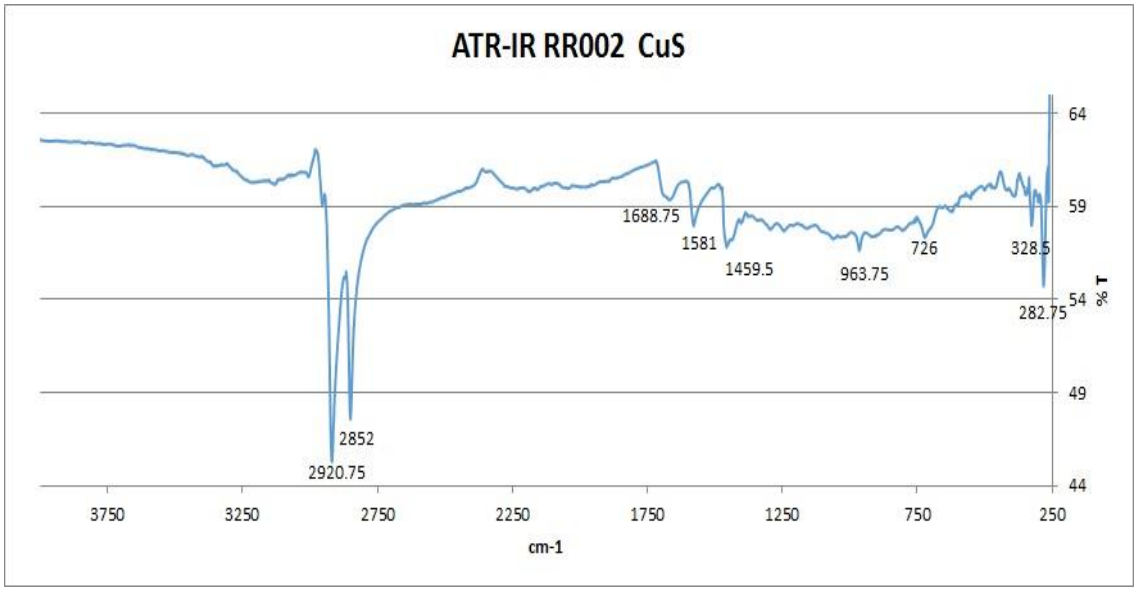

Figure 32: ATR -FTIR CuS nanoplates (product 1)

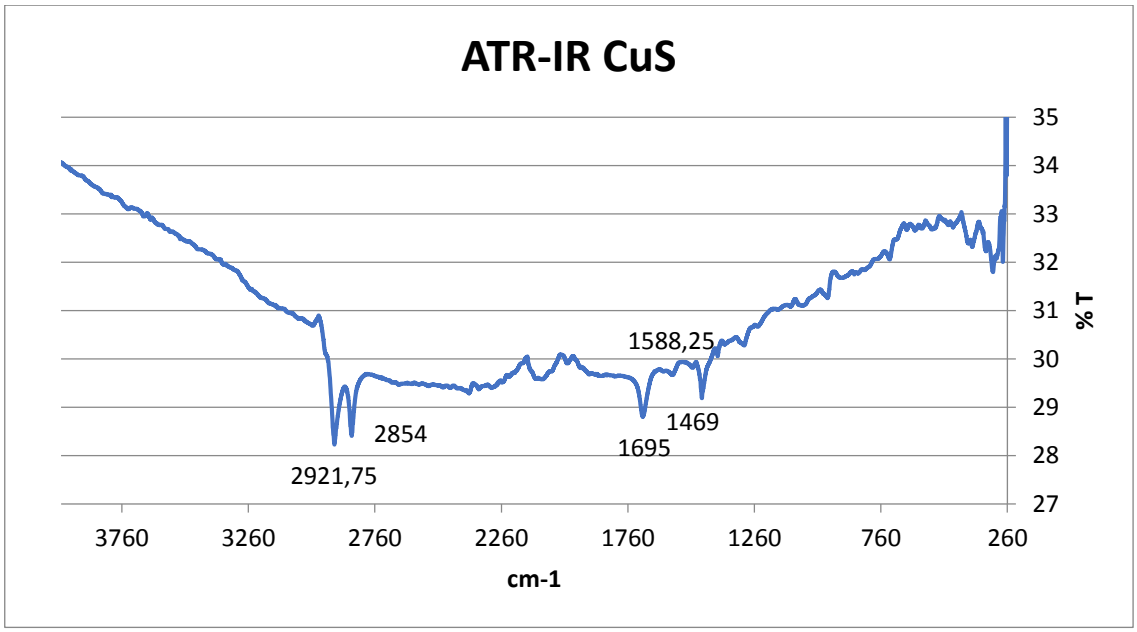

Figure 33: ATR-IR CuS nanoplates (product 2)

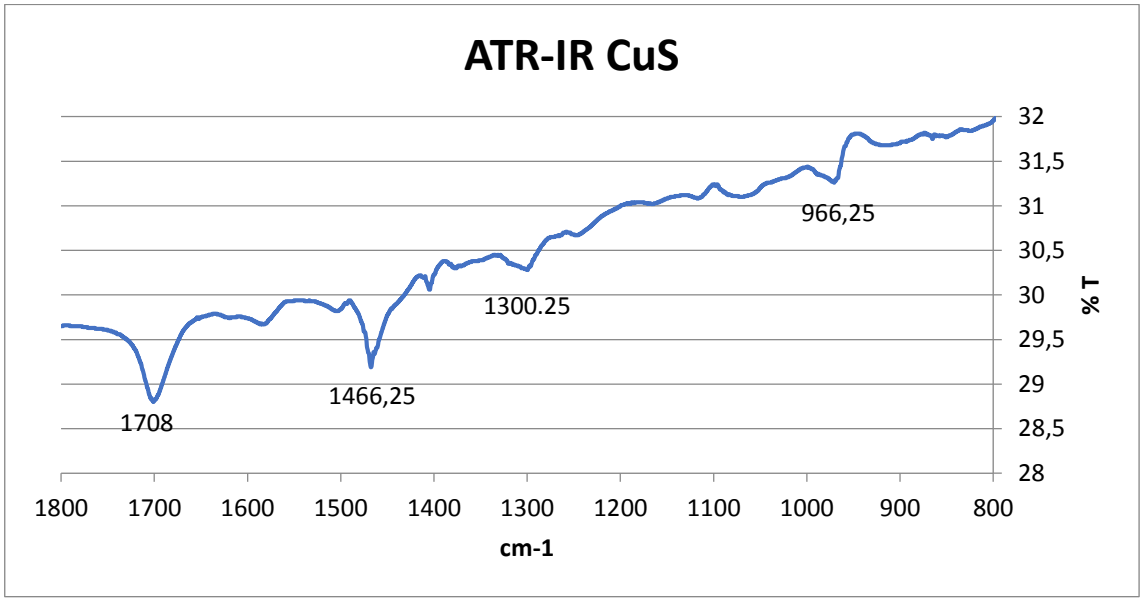

Figure 34: ATR-FTIR CuS nanoplates (product 2)

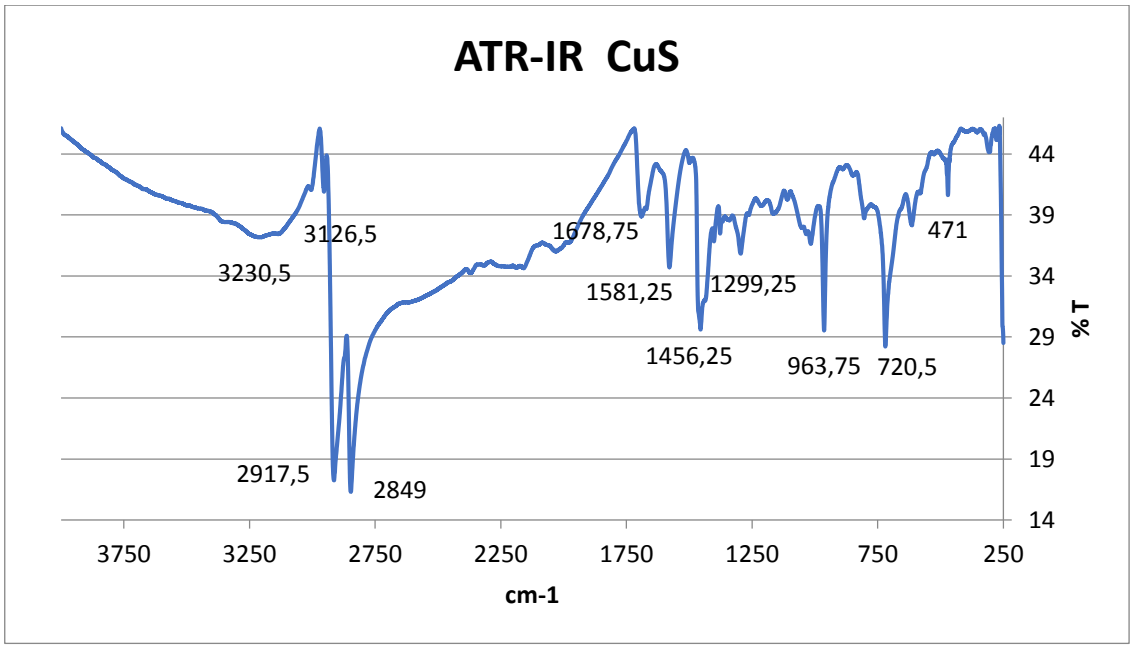

Figure 35: ATR-IR CuS (product 3)

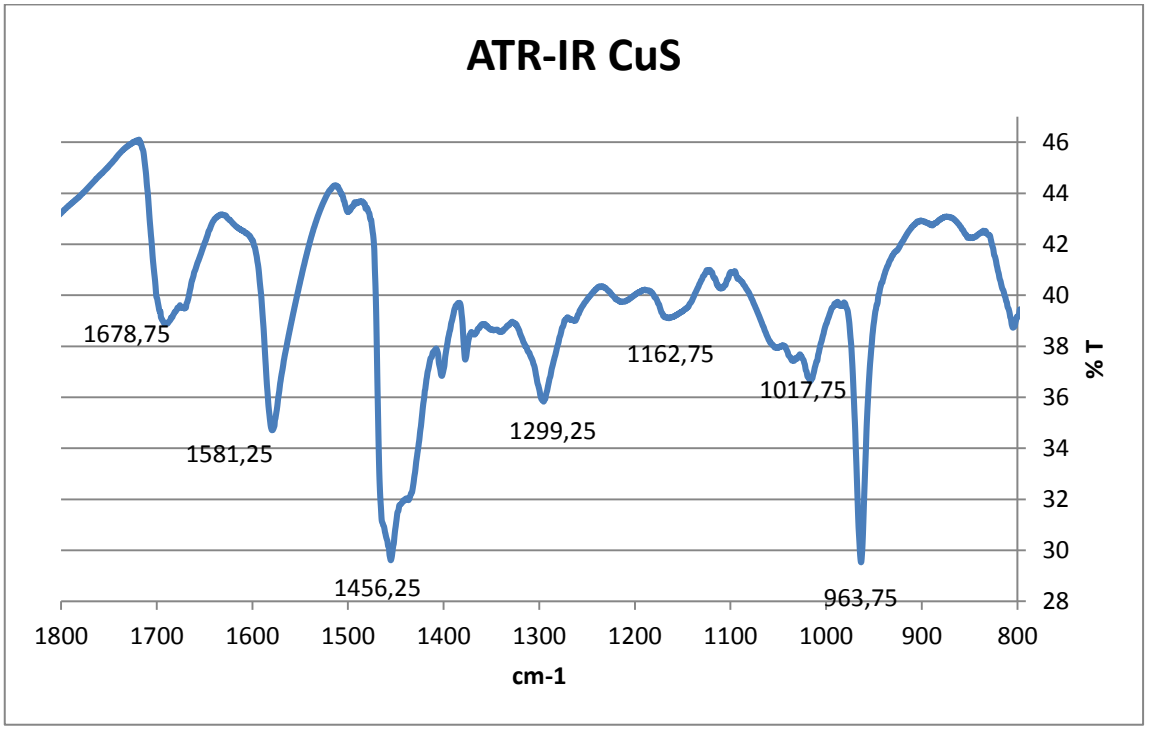

Figure 36: ATR-IR CuS nanoplates (product 3)

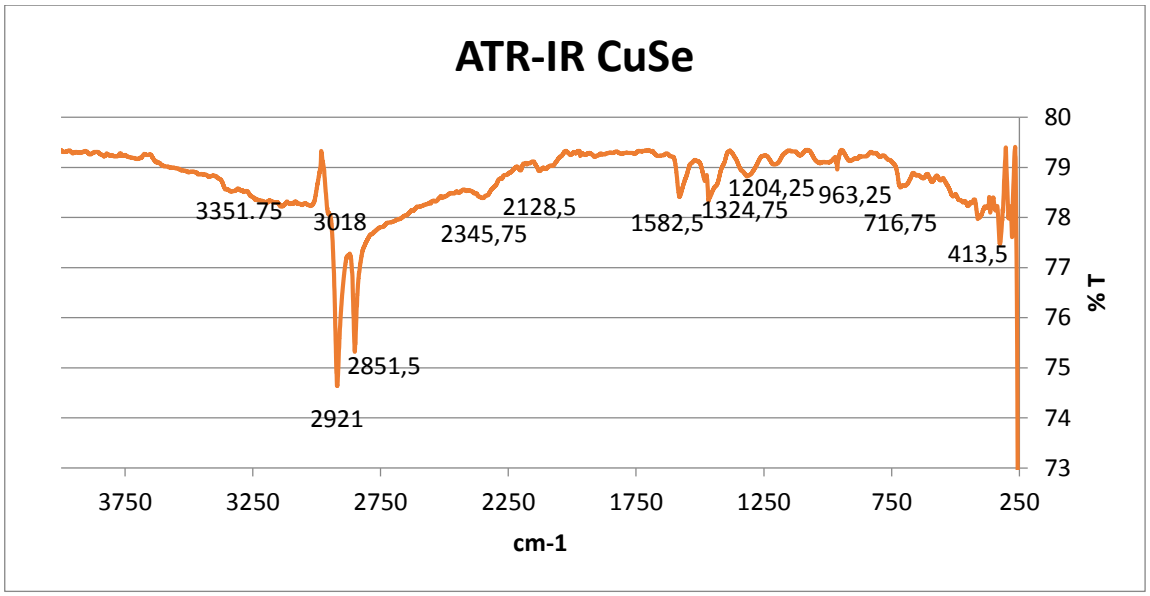

Figure 37: ATR-IR CuSe (product 1)

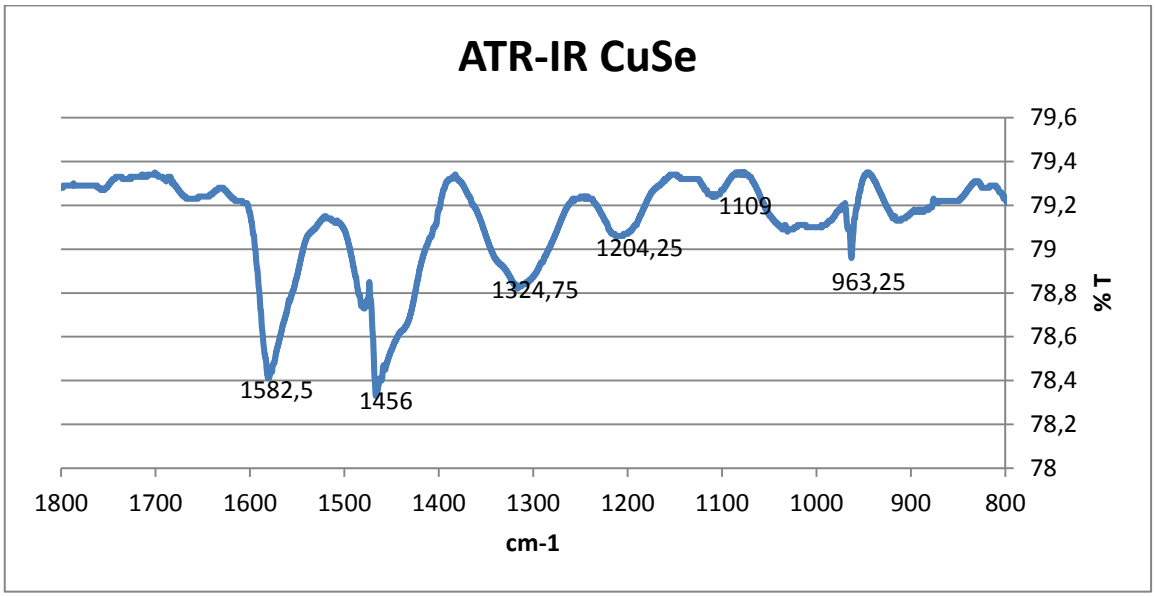

Figure 38: ATR-FTIR CuSe (product 1)

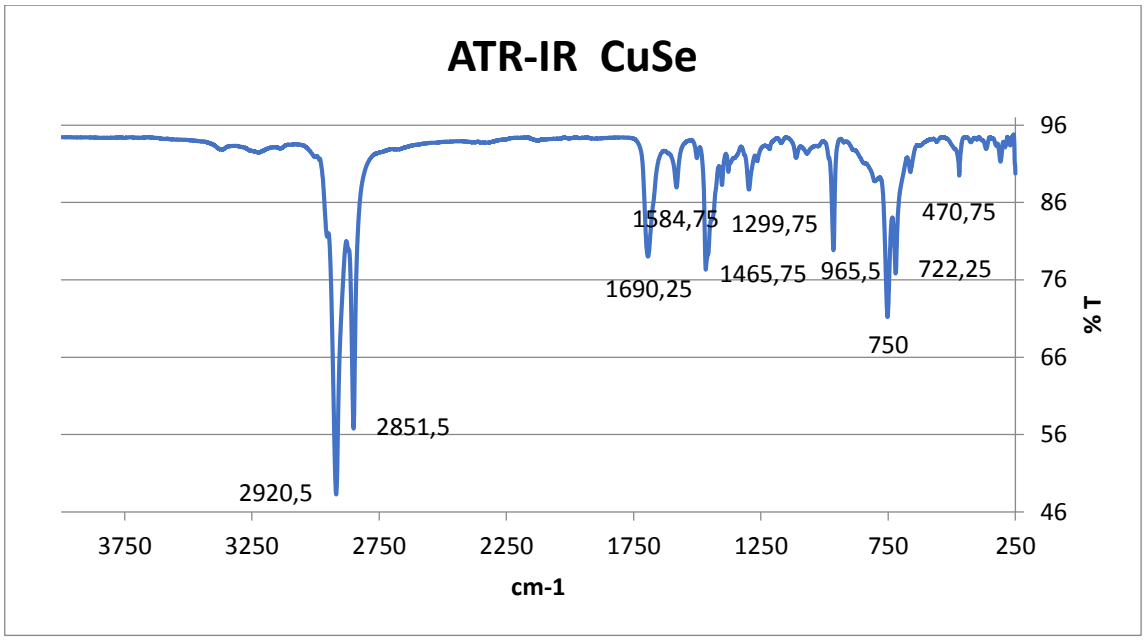

Figure 39: ATR-IR CuSe (product 2)

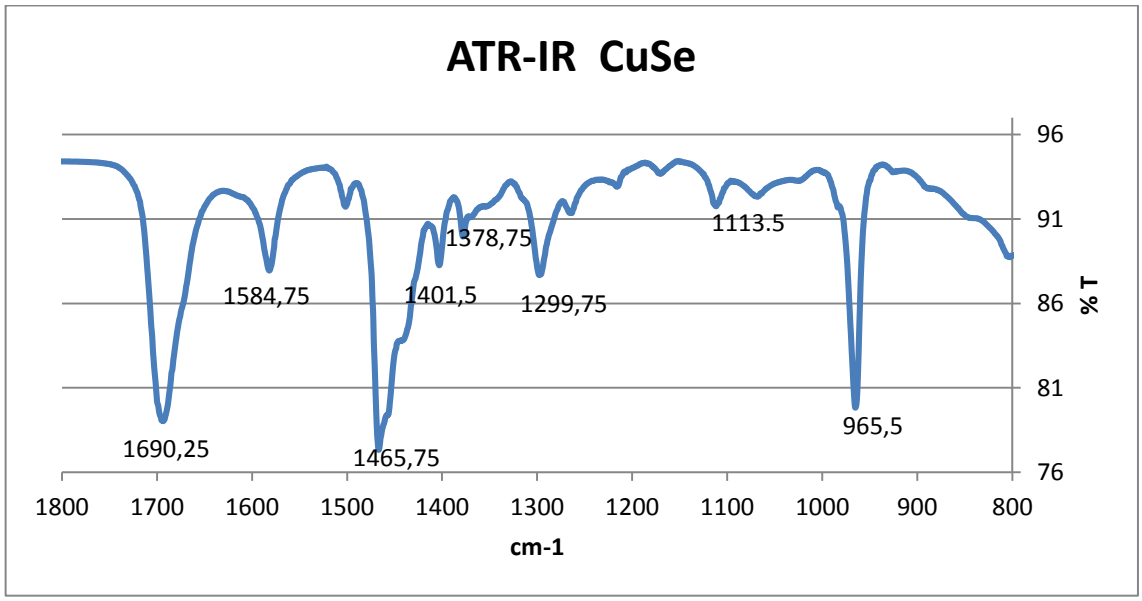

Figure 40: AT-IR CuSe nanoplates (product 2)

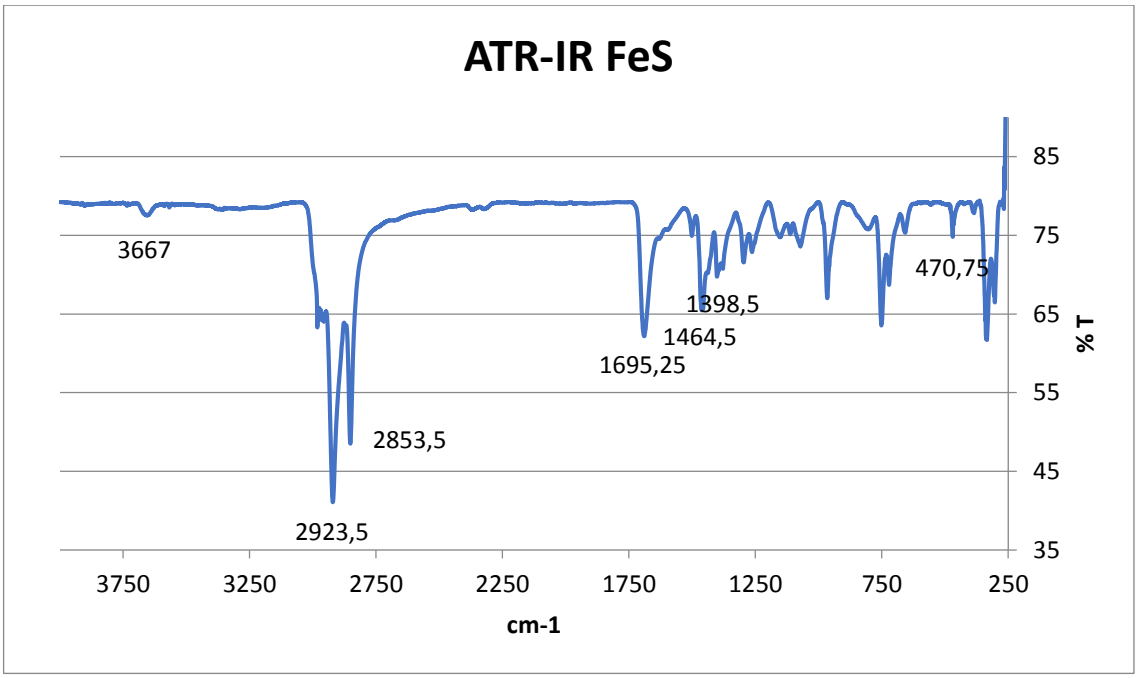

Figure 41: ATR-IR Fe(III)S

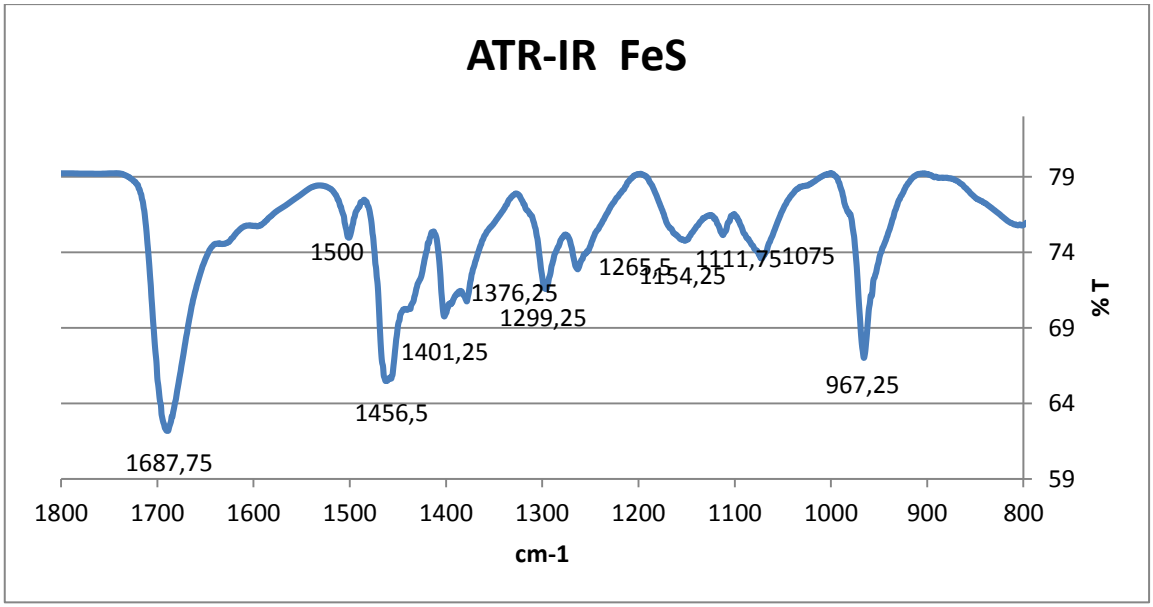

Figure 42: ATR-IR Fe(III)S nanosheets

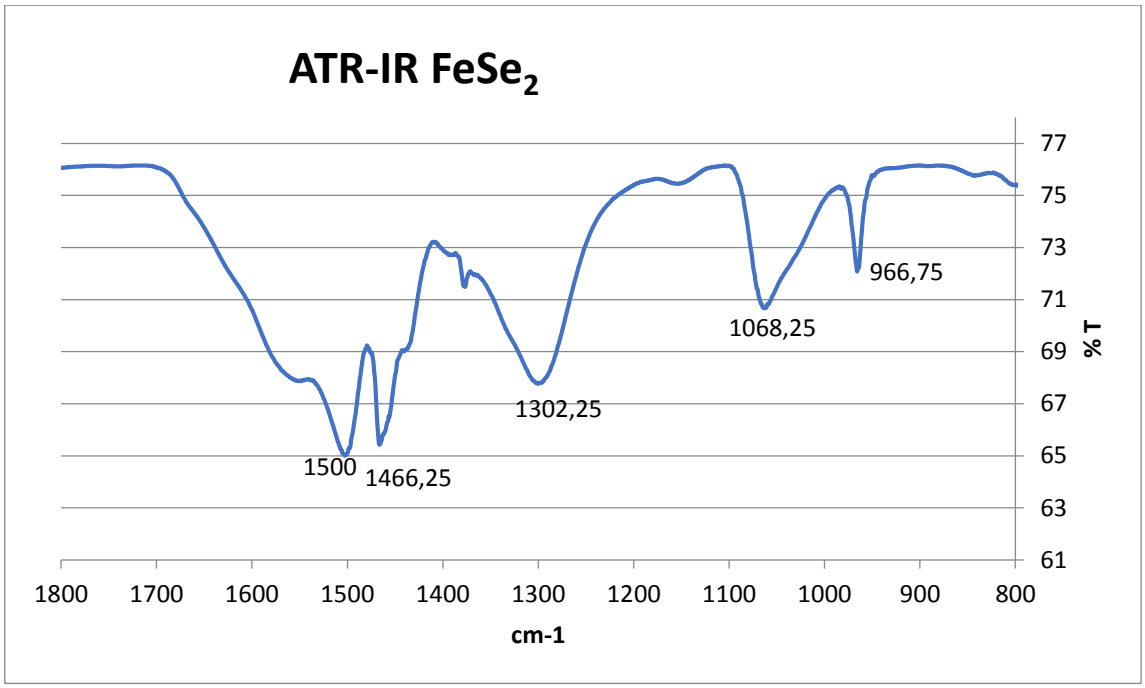

Figure 43: ATR-IR $FeSe_2$

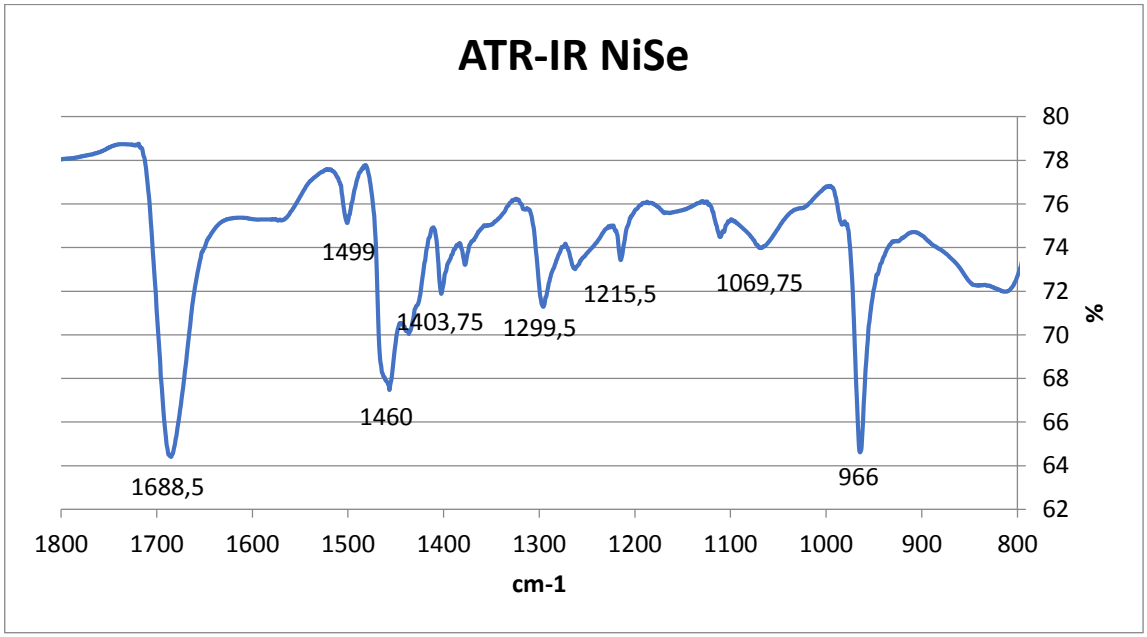

Figure 44: ATR IR NiSe

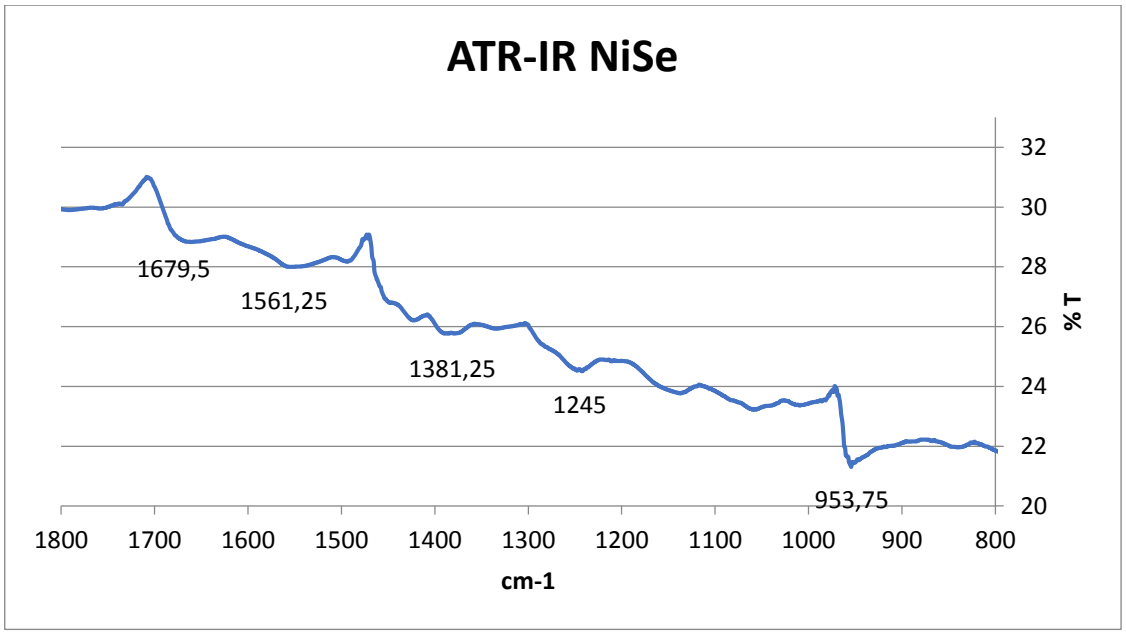

Figure 45: ATR-IR NiSe nanoscrolls